**RC22734 (W0303-005) March 3, 2003**
**Physics**

# IBM Research Report

## Reduction of the Electron Mobility in High-k MOS Systems caused by Remote Scattering with Interfacial Optical Phonons

**Massimo V. Fischetti, Deborah Neumayer, Eduard Cartier**
IBM Research Division
Thomas J. Watson Research Center
P.O. Box 218
Yorktown Heights, NY 10598

**Research Division**
**Almaden - Austin - Beijing - Delhi - Haifa - India - T. J. Watson - Tokyo - Zurich**

**LIMITED DISTRIBUTION NOTICE**: This report has been submitted for publication outside of IBM and will probably be copyrighted if accepted for publication. It has been issued as a Research Report for early dissemination of its contents. In view of the transfer of copyright to the outside publisher, its distribution outside of IBM prior to publication should be limited to peer communications and specific requests. After outside publication, requests should be filled only by reprints or legally obtained copies of the article (e.g. , payment of royalties). Copies may be requested from IBM T. J. Watson Research Center ,
P. O. Box 218, Yorktown Heights, NY 10598 USA (email: reports@us.ibm.com). Some reports are available on the internet at http://domino.watson.ibm.com/library/CyberDig.nsf/home .

# REDUCTION OF THE ELECTRON MOBILITY IN HIGH-$\kappa$ MOS SYSTEMS CAUSED BY REMOTE SCATTERING WITH SOFT INTERFACIAL OPTICAL PHONONS

Massimo. V. Fischetti[1], Deborah A. Neumayer[1], and Eduard A. Cartier[1,2]

[1]IBM Semiconductor Research and Development Center (SRDC)
IBM Research Division, Thomas J. Watson Research Center
P. O. Box 218, Yorktown Heights, NY 10598, USA
[2] International Sematech Assigneee at IMEC, Kepeldreef 75, B-3001 Leuven, Belgium

The poor electron mobility presently observed in metal-insulator-semiconductor devices using high-$\kappa$ insulators may be due to a variety of processing and material-related issues. However, here we argue that the high-$\kappa$ itself may present an intrinsic, unavoidable cause of this poor performance. Indeed, the high dielectric constant is usually accompanied by the presence of soft optical phonons. The long-range dipole field associated with the interface excitations, while small in the case of $SiO_2$, for most high-$\kappa$ materials is sufficiently large to depress the effective electron mobility in the inversion layer of the Si substrate. We study the dispersion of the interfacial coupled phonon-plasmon modes, their electron-scattering strength, and their effect on the electron mobility for Si-gate structures employing films of $SiO_2$, $Al_2O_3$, AlN, $ZrO_2$, $HfO_2$, and $ZrSiO_4$ for '$SiO_2$-equivalent' thicknesses ranging from 5 nm to 0.5 nm.

## I. INTRODUCTION

Insulators with a large static dielectric constant (usually referred to as 'high-$\kappa$ insulators) are presently being considered as possible replacements for $SiO_2$, because of the necessity of increasing the gate capacitance of Si metal-oxide-semiconductor field-effect transistors (MOSFETs), while avoiding the problems which arise when the $SiO_2$ thickness is reduced below the 1.5-1.0 nm range, as demanded by device scaling[1,2]. At least at present, these efforts are still mainly aimed at improving the chemical and physical properties of the insulating materials. Yet, in this paper we point out an intrinsic, possibly unavoidable, and unwanted property of these materials, namely, the fact that their high dielectric constant may necessarily cause a reduction of the electron mobility in the inversion layer of Si MOSFETs. The dielectric constant of a (non metallic) solid results from the contribution of the ionic and the electronic polarization. The latter is roughly inversely proportional to the square of the direct band gap of the solid, averaged over the Brillouin Zone. Insulators, by definition, have large band-gaps, so that there is little one can do to increase the electronic polarization and a larger (static) dielectric constant can only stem from a larger ionic polarization, often due to highly polarizable ('soft') metal-oxygen bonds. Associated with soft bonds are low-energy optical phonons. By contrast, the 'hard' Si-O bonds in $SiO_2$ yield a reduced ionic polarization. Associated with 'hard' bonds are 'stiff' optical phonons.

In 1972, Wang and Mahan[3] showed that electrons in the inversion layer at the interface between a semiconductor of optical permittivity $\epsilon_s^\infty$ and a dielectric of static and optical permittivities $\epsilon_{ox}^0$ and $\epsilon_{ox}^\infty$, respectively, can couple with the surface-optical (SO) modes (arising at the insulator/Si interface from the longitudinal-optical (LO) modes of the insulator) with a coupling strength proportional to

$$\hbar\omega_{SO} \left[ \frac{1}{\epsilon_s^\infty + \epsilon_{ox}^\infty} - \frac{1}{\epsilon_s^\infty + \epsilon_{ox}^0} \right] . \quad (1)$$

Here $\hbar$ is the reduced Planck constant and $\omega_{SO}$ is the frequency of the SO insulator-phonon, given by:

$$\omega_{SO} = \omega_{TO} \left[ \frac{\epsilon_{ox}^0 + \epsilon_{Si}^\infty}{\epsilon_{ox}^\infty + \epsilon_{Si}^\infty} \right]^{1/2} . \quad (2)$$

Equation (1) is physically equivalent to the well-known Fröhlich electron/LO-phonon scattering strength, proportional to

$$\hbar\omega_{LO} \left[ \frac{1}{\epsilon^\infty} - \frac{1}{\epsilon^0} \right] , \quad (3)$$

in a material with static and optical permittivities $\epsilon^0$ and $\epsilon^\infty$, respectively, and LO-phonon frequency $\omega_{LO}$. In Eq. (3) the difference between the inverse of $\epsilon^0$ and of $\epsilon^\infty$ is proportional to the squared-amplitude of the dipole field solely due to the oscillating ionic polarization of the material; that is, to the coupling between electrons and the bulk LO-phonons. Equation (1) results from the same physics, but the dipole field is modified by 'image-charge effects' at the insulator/semiconductor interface, affecting the decay of the dipole field of the insulator-phonons away from the bulk of the insulator into the semiconductor inversion layer. The effect of this scattering mechanism, called 'remote phonon scattering', on hot-electron transport in the Si/$SiO_2$ system was later studied by Hess and Vogl[4] and by Moore and Ferry[5], and its effect on the effective

electron mobility by one of us (MVF)[6]. For the $Si/SiO_2$ system, and restricting our attention – now and throughout the rest of the paper – to the electron mobility, remote scattering does not play a major role. There are two reasons for this. First, the ionic polarizability of $SiO_2$ is not very large, because of the hard nature of the Si-O bond. While this results in a small static dielectric constant, it also results in a small difference between $\epsilon_{ox}^{0}$ and $\epsilon_{ox}^{\infty}$, and so in a small coupling constant for electron/remote-phonon scattering. Second, the stiff Si-O bond also results in a large LO (and SO) phonon energy ($\hbar\omega_{LO} \approx 0.15$ eV). Electrons at thermal energies (which should be considered when interested in their Ohmic mobility) cannot emit excitations of such a large energy, and at room temperature there are too few thermally-excited phonons to be absorbed. Note that another bulk $SiO_2$ phonon with $\hbar\omega_{LO} \approx 63$ meV could potentially have a larger effect, as far as these energetic considerations are concerned, but its oscillator strength is too small: If it were not so, $SiO_2$ would have a significantly larger $\kappa$.

Considering now the case of high-$\kappa$ insulators, their high-frequency dielectric response is mainly electronic – since heavier and 'slower' ions cannot respond fully at sufficiently large frequencies –and so it is not too different from that of $SiO_2$. On the contrary, the large ionic response dominates at low frequency. This does indeed yield a larger static dielectric constant, but also yields both a large difference between $\epsilon_{ox}^{0}$ and $\epsilon_{ox}^{\infty}$, and so in a large scattering strength, Eq. (1), and in a low SO-phonon frequency, which allows frequent emissions and absorption processes by thermal electrons. The net result is that the very same physical properties which are responsible for the higher $\kappa$ of the insulator are also likely to yield (with some important exceptions we shall consider later) a degradation of the effective electron mobility in the inversion layer of MOS-systems using the high-$\kappa$ insulator. We should remark that there is nothing novel about these arguments: Hess and Vogl[4] were already very well aware of these ideas in 1979, when they concluded their article with the optimistic remark: *"In passing, we note that a reduction of the ionic polarizability of $SiO_2$, or better of the difference $\epsilon_{ox}^{0} - \epsilon_{ox}^{\infty}$, would reduce the electron-phonon coupling,* [...] *and correspondingly, enhance the field dependent electron mobility in MOS transistors"*. Unfortunately in our context we must move in the opposite direction, from $SiO_2$ to higher-$\kappa$ materials with a higher difference $\epsilon_{ox}^{0} - \epsilon_{ox}^{\infty}$, thus achieving the opposite effect of depressing the mobility.

It is instructive to start by giving a rough idea about the size of the effect we are considering. In Fig. 1 we plot the effective electron mobility in the inversion layer at the interface between Si and an infinitely-thick film of several insulators we have considered ($SiO_2$, $HfO_2$, $ZrO_2$, $ZrSiO_4$, AlN, and $Al_2O_3$). Full details will be given below. For now it suffices to say that the triangular well approximation has been used to treat the inversion layer, an anisotropic and nonparabolic band-structure model has been used to account for (anisotropic) scattering with acoustic phonons, as described in Ref. 7, surface roughness has been accounted for empirically using Matthiessen's rule, and scattering with remote SO modes has been treated using Fermi's Golden Rule with the Wang-Mahan matrix element proportional to the scattering strength given in Eq. (1). While this model is excessively oversimplified for the reasons stated below, it shows that effects as large as a factor of 2 or more can be expected.

In principle, the results shown in Fig. 1 are only suggestive of what we should expect. A more accurate assessment of the the importance of remote phonon scattering in realistic high-$\kappa$ MOS systems requires that we account for two additional complications: the coupling between surface/interface optical modes and the two-dimensional electron plasma at the insulator/semiconductor interface, and the coupling between interfacial optical and plasma modes at the substrate/insulator and at the gate/insulator inter-

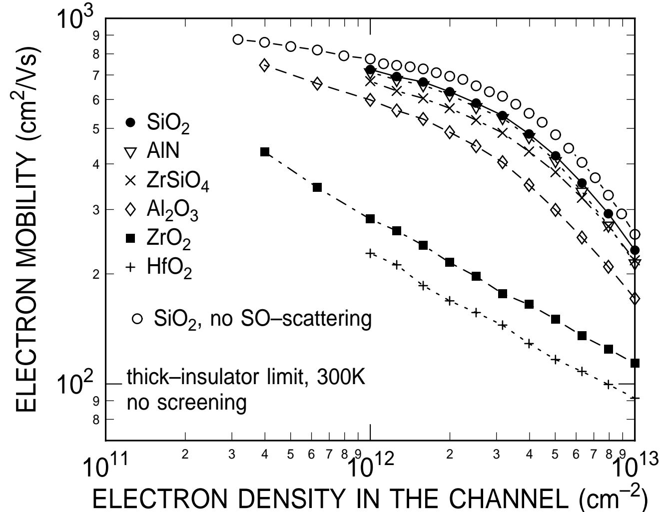


**Fig.** 1: Effective electron mobility in Si inversion layers of MOS systems with the insulators indicated. A triangular well approximation has been used to model the subband structure of the inversion layer. Anisotropic scattering with acoustic phonons and remote scattering with surface optical phonons has been accounted for (when indicated). Scattering with surface roughness has been added empirically using Matthiessen's rule and fitting the roughness-parameters to match the experimental 'universal' mobility for the Si/$SiO_2$ system at an electron sheet density of $10^{13}$ $cm^{-2}$. The limit of infinite insulator thickness has been taken, and no additional dielectric effects (screening by substrate and gate electrons, plasmon-phonon coupling) have been considered here.

faces. In thin-insulator structures this coupling alters significantly the dispersion of the excitations and their coupling with the electrons in the channel. The coupling between substrate- and gate-interface plasmons has been investigated before, finding that a significant gate Coulomb-drag yields by itself a reduction of the electron mobility for $SiO_2$ layers thinner than about 2-1.5 nm.[7] Here we must extend the treatment by including the coupling of surface plasmons to surface-optical modes, by accounting for electron scattering with the resulting phonon-like modes, and considering MOS systems with various thickness of different insulators of practical technological importance. Anticipating our main result, the proximity of the heavily-doped gate has the beneficial effect of screening to a large extent the interaction between electrons and interface optical modes at the smallest insulator thickness considered for all but two ($HfO_2$ and $ZrO_2$) of the high-$\kappa$ insulators we have considered, and at sufficiently large electron density in the depleted poly-Si gate.

This chapter is organized as follows: In Sec. II we present our theoretical scheme. In Sec. III we present our results. In particular, Sec. III.B presents a discussion of the non-trivial problem of selecting physical quantities (LO and/or transverse-optical, or TO, phonon energies, dielectric constants, and oscillator strengths) of the insulating films, comparing information available in the literature with data extracted from Fourier Transform InfraRed (FTIR) Spectroscopy. Finally, in Sec. IV we present some estimates about the role played by an interfacial $SiO_2$ layer and conclude in Sec. V. The role of remote phonon scattering on hot-electron (*i.e.* non Ohmic) transport will not be investigated here, although we should expect significant effects, along the line of a previous investigation of long-range Coulomb effects on the transconductance of Si $n$-MOSFETs (Ref. 8).

## II. INTERFACE MODES

### A. Dispersion

Here, as in Ref. 7, we shall consider a structure consisting of degenerately-doped $n$-type Si (representing the poly-Si gate) in the half-space $z < 0$ (gate), an $SiO_2$ or high-$\kappa$ insulating layer for $0 \leq z < t$, and a $p$-type Si substrate filling the half-space $z \geq t$. The latter is assumed to be electrically inverted, and so it is treated as a two-dimensional electron gas (2DEG). We shall denote by $\epsilon_g(\omega)$, $\epsilon_{ox}(\omega)$, and $\epsilon_s(Q,\omega)$ the dielectric functions of the gate, insulator, and substrate, respectively (all in the long-wavelength limit discussed below). We denote by $\mathbf{Q}$ and $\mathbf{R}$ the two-dimensional wave vector and coordinate-vector in the $(x,y)$-plane of the interfaces, respectively.

We are only interested in the longitudinal electric eigenmodes of the system, since transverse modes (given by poles of the total dielectric response) correspond to a vanishing electric field, and so to a vanishing coupling with the charge carriers. These are transverse-magnetic solutions (TM- or $p$-waves) of Maxwell's equations. As described in Ref. 7, we can safely work in the non-retarded limit. Thus, the 'usual' boundary conditions require that the components of the electric field on the plane of the interfaces be continuous across the two interfaces at $z = 0$ and $z = t$, and similarly for the component of the displacement field normal to the plane of the interfaces. We can expand the electrostatic potential at frequency $\omega$ in its Fourier components as:

$$\phi(\mathbf{R},z,t) \; = \; \sum_{\mathbf{Q}} \; \phi_{Q,\omega}(z) \; e^{i\mathbf{Q}\cdot\mathbf{R}} \; e^{i\omega t} \; . \tag{4}$$

Here and in the following it must be understood that only the real part of the complex exponentials must be retained. Assuming an isotropic dielectric response everywhere, and thanks to the cylindrical symmetry of the problem, $\phi_{Q,\omega}(z)$ depends only on the magnitude of the wave vector $\mathbf{Q}$. Thus, we are led to finding the solution of the Laplace equation which in Fourier space reads as:

$$\frac{d^2\phi_{Q,\omega}(z)}{dz^2} - Q^2\phi_{Q,\omega}(z) \; = \; 0 \; . \tag{5}$$

The boundary conditions at the interfaces imply that a physically acceptable solution of Eq. (5) exists provided we satisfy the secular equation:

$$\epsilon_{ox}(\omega)^2 \; + \; \epsilon_{ox}(\omega)[\epsilon_g(\omega) + \epsilon_s(Q,\omega)] \; \mathrm{cotanh}(Qt) \; + \; \epsilon_g(\omega)\epsilon_s(Q,\omega) \; = \; 0 \; . \tag{6}$$

The solutions of this equation yield the dispersion of the modes, $\omega(Q) = \omega_Q^{(i)}$, where the index $i$ runs over the branches of the modes. The solution $\phi_{Q,\omega}(z)$ has the form:

$$\phi_{Q,\omega_Q^{(i)}}(z) \; = \; \begin{cases} a_{Q,\omega_Q^{(i)}} \; e^{Qz} & (z < 0) \\ b_{Q,\omega_Q^{(i)}} \; e^{-Qz} + c_{Q,\omega_Q^{(i)}} \; e^{Qz} & (0 \leq z < t) \\ d_{Q,\omega_Q^{(i)}} \; e^{-Qz} & (z \geq t) \end{cases} \; , \tag{7}$$

where:

$$b_{Q,\omega_Q^{(i)}} \; = \; \frac{\epsilon_{ox}(\omega_Q^{(i)}) - \epsilon_g(\omega_Q^{(i)})}{2\epsilon_{ox}(\omega_Q^{(i)})} \; a_{Q,\omega_Q^{(i)}} \; , \tag{8}$$

$$c_{Q,\omega_Q^{(i)}} = \frac{\epsilon_{ox}(\omega_Q^{(i)}) + \epsilon_g(\omega_Q^{(i)})}{2\epsilon_{ox}(\omega_Q^{(i)})} \, a_{Q,\omega_Q^{(i)}} \ , \tag{9}$$

$$d_{Q,\omega_Q^{(i)}} = \frac{\epsilon_{ox}(\omega_Q^{(i)}) - \epsilon_g(\omega_Q^{(i)})}{\epsilon_{ox}(\omega_Q^{(i)}) + \epsilon_s(Q,\omega_Q^{(i)})} \, a_{Q,\omega_Q^{(i)}} \ , \tag{10}$$

The determination of multiplicative constant $a_{Q,\omega_Q^{(i)}}$ will be discussed below in Sec. II.B.

The selection of a model dielectric-response for the insulator is a quite delicate issue. In principle, we should account for polarization effects due to a multitude of optical modes, functions not only of the chosen materials, but also of their chemical composition (stoichiometric or not, depending on deposition and annealing conditions), on their allotropic forms (amorphous or, if crystalline, on their crystallographic structure), etc. In order to keep the model tractable, we consider only two bulk optical modes, obtained by averaging over direction (*e.g.*, over the $A_{2u}$ and $E_u$ modes for bc tetragonal $ZrO_2$ or $ZrSiO_4$), by considering only the two modes exhibiting the largest oscillator strength, by lumping 'bands' of modes into two groups, or by combining of all of these approximations.[9] Thus, we assume an ionic dielectric function of the 'oscillator' form:

$$\epsilon_{ox}(\omega) = \epsilon_{ox}^{\infty} + (\epsilon_{ox}^{i} - \epsilon_{ox}^{\infty}) \frac{\omega_{TO2}^2}{\omega_{TO2}^2 - \omega^2} + (\epsilon_{ox}^{0} - \epsilon_{ox}^{i}) \frac{\omega_{TO1}^2}{\omega_{TO1}^2 - \omega^2} \ , \tag{11}$$

where $\epsilon_{ox}^0$ and $\epsilon_{ox}^\infty$ are the static and optical permittivity of the insulator, respectively, (so that $\kappa = \epsilon_{ox}^0/\epsilon_0$, where $\epsilon_0$ is the permittivity of vacuum) and $\omega_{TO1}$ and $\omega_{TO2}$ are the angular frequencies of the only two TO-phonon modes we shall consider in the insulator. We assume $\omega_{TO1} \leq \omega_{TO2}$. Finally, $\epsilon_{ox}^i$ is the insulator permittivity describing the dielectric response at some intermediate frequency $\omega_{int}$ such that $\omega_{TO1} \leq \omega_{int} \leq \omega_{TO2}$. Physically, it is related to the oscillator strength of each mode and it must be determined from the energy splitting between longitudinal and transverse optical modes via the Lyddane-Sachs-Teller relation (or its trivial extension in the case of two optical modes), which allows us to rewrite Eq. (11) as:

$$\epsilon_{ox}(\omega) = \epsilon_{ox}^{\infty} \frac{(\omega_{LO2}^2 - \omega^2)(\omega_{LO1}^2 - \omega^2)}{(\omega_{TO2}^2 - \omega^2)(\omega_{TO1}^2 - \omega^2)} \ , \tag{12}$$

where the frequency of the two LO-modes is given by the generalized Lyddane-Sachs-Teller relation:

$$\omega_{LOi}^2 = \frac{1}{2\Delta} \left[ b \pm (b^2 - 4\Delta c)^{1/2} \right] \qquad (i = 1, 2) \ , \tag{13}$$

with:

$$\begin{aligned} \Delta &= \epsilon_{ox}^{\infty} \\ b &= \Delta(\omega_{TO1}^2 + \omega_{TO2}^2) + (\epsilon_{ox}^{i} - \epsilon_{ox}^{\infty})\, \omega_{TO2}^2 + (\epsilon_{ox}^{0} - \epsilon_{ox}^{i})\, \omega_{TO1}^2 \\ c &= (\Delta + \epsilon_{ox}^{0} - \epsilon_{ox}^{\infty})\, \omega_{TO1}^2 \omega_{TO2}^2 \ . \end{aligned} \tag{14}$$

For the electronic response of the gate we take the usual long-wavelength expression:

$$\epsilon_g(\omega) = \epsilon_{Si}^{\infty} \left( 1 - \frac{\omega_{p,g}^2}{\omega^2} \right) \ , \tag{15}$$

where $\omega_{p,g}^2 = e^2 N_g/(\epsilon_{Si}^{\infty} m_g)$ is the bulk plasma frequency of the polycrystalline-Si gate with an electron density $N_g$ (obtained from some suitable average of the electron

density over the depletion layer of the poly-Si gate, as discussed below in Sec. III.A), with an effective mass $m_g$ ($= 0.32\ m_0$, where $m_0$ is the electron mass), and optical permittivity $\epsilon_{Si}^{\infty}$. Finally, for the inverted substrate we assume:

$$\epsilon_s(Q,\omega) \ = \ \epsilon_{Si}^{\infty} \left[ 1 \ - \ \frac{\omega_{p,s}(Q)^2}{\omega^2} \right] \ , \tag{16}$$

where $\omega_{p,s}(Q)^2 \ = \ [\sum_\nu e^2 n_\nu Q/(\epsilon_{Si}^{\infty} m_\nu)]^{1/2}$ is the plasma frequency of the 2DEG, $n_\nu$ and $m_\nu$ being the electron density and conductivity mass in each of the occupied subbands labeled by the index $\nu$.

Equation (6) is an algebraic equation of sixth degree in $\omega^2$, and which we shall label its six positive solutions as $\omega_Q^{(i)}$. Two of these solutions (which we shall label with the indices $i = 5, 6$) are associated with a small scattering field and will be ignored. Indeed, for small values of $Qt$, they behave like bulk TO-modes and couple poorly with the electrons in the inversion layer. At large values of $Qt$, instead, they are mainly localized at the 'far' gate/insulator interface – thus yielding a scattering strength depressed by a factor $\sim e^{-2Qt}$ – , with frequencies approaching the frequencies of the bare SO modes at that interface. The remaining 4 solutions (which we shall label with the index $i$ running from 1 through 4, ordered so that $\omega_Q^{(1)} \geq \omega_Q^{(2)} \geq \omega_Q^{(3)} \geq \omega_Q^{(4)}$) represent coupled interface plasmon-phonon modes.

Two issues regarding these modes must be addressed before we can evaluate their scattering strength: How to estimate their separate phonon- and plasmon-content, and how to handle them in a regime in which Landau damping dominates.

The first issue can be addressed by extending the result of Kim and coworkers[11] to the case of interest here. The gate-plasmon content of mode $i$ will be defined as:

$$\Pi^{(G)}(\omega_Q^{(i)}) \ \approx \ \left| \frac{(\omega_Q^{(i)2} - \omega_Q^{(-g,1)2})\ (\omega_Q^{(i)2} - \omega_Q^{(-g,2)2})\ (\omega_Q^{(i)2} - \omega_Q^{(-g,3)2})}{(\omega_Q^{(i)2} - \omega_Q^{(j)2})\ (\omega_Q^{(i)2} - \omega_Q^{(k)2})\ (\omega_Q^{(i)2} - \omega_Q^{(l)2})} \right| \ , \tag{17}$$

where the indices $(i,j,k,l)$ are cyclical. The 'approximate' sign above results from having neglected the two solutions mentioned above. Similarly, considering the three solutions $\omega_Q^{(-s,\alpha)}$) ($\alpha = 1, 3$), obtained from the secular equation Eq. (6) by ignoring the plasma response of the 2DEG in the substrate (that is, by replacing $\epsilon_s(Q,\omega)$ with $\epsilon_{Si}^{\infty}$), we define the substrate-plasmon content of mode $i$ as:

$$\Pi^{(S)}(\omega_Q^{(i)}) \ \approx \ \left| \frac{(\omega_Q^{(i)2} - \omega_Q^{(-s,1)2})\ (\omega_Q^{(i)2} - \omega_Q^{(-s,2)2})\ (\omega_Q^{(i)2} - \omega_Q^{(-s,3)2})}{(\omega_Q^{(i)2} - \omega_Q^{(j)2})\ (\omega_Q^{(i)2} - \omega_Q^{(k)2})\ (\omega_Q^{(i)2} - \omega_Q^{(l)2})} \right| \ . \tag{18}$$

It can be verified that Eqns. (17) and (18) satisfy the normalization conditions:

$$\sum_{i=1}^{4} \Pi^{(G)}(\omega_Q^{(i)}) \ = 1 \ , \qquad \sum_{i=1}^{4} \Pi^{(S)}(\omega_Q^{(i)}) \ = 1 \ . \tag{19}$$

Having ignored the solutions $\omega_Q^{(5)}$ and $\omega_Q^{(6)}$ forces us to approximate the phonon content of each mode as follows. From Eqns. (17) and (18) it follows that the total phonon content of mode $i$ will be:

$$\Phi(\omega_Q^{(i)}) \ = 1 \ - \Pi^{(G)}(\omega_Q^{(i)}) \ - \Pi^{(S)}(\omega_Q^{(i)}) \ . \tag{20}$$

In order to define separate phonon-1 and phonon-2 contents, we also consider the three solutions $\omega_Q^{(-TO1,\alpha)}$ ($\alpha = 1,3$), obtained from the secular equation, Eq. (6), but now ignoring the response of phonon-1 – that is, by replacing $\epsilon_{ox}(\omega)$ with $\epsilon_{ox}^{\infty}(\omega_{LO2}^2 - \omega^2)/(\omega_{TO2}^2 - \omega^2)$ – and the three solutions $\omega_Q^{(-TO2,\alpha)}$ ($\alpha = 1,3$) similarly obtained by ignoring the response of the TO-mode 2 by setting in Eq. (6) $\epsilon_{ox}(\omega) \to \epsilon_{ox}^{\infty}(\omega_{LO1}^2 - \omega^2)/(\omega_{TO1}^2 - \omega^2)$. Therefore, the relative phonon-1 content of mode $i$ will be

$$R^{(TO1)}(\omega_Q^{(i)}) \approx \left| \frac{(\omega_Q^{(i)^2} - \omega_Q^{(-TO1,1)^2})\ (\omega_Q^{(i)^2} - \omega_Q^{(-TO1,2)^2})\ (\omega_Q^{(i)^2} - \omega_Q^{(-TO1,3)^2})}{(\omega_Q^{(i)^2} - \omega_Q^{(j)^2})\ (\omega_Q^{(i)^2} - \omega_Q^{(k)^2})\ (\omega_Q^{(i)^2} - \omega_Q^{(l)^2})} \right| , \quad (21)$$

(where, as before, $i, j, k, l$ are cyclical) so that, finally, the TO-phonon-1 content of mode $i$ will be:

$$\Phi^{(TO1)}(\omega_Q^{(i)}) \approx \frac{R^{(TO1)}(\omega_Q^{(i)})}{R^{(TO1)}(\omega_Q^{(i)}) + R^{(TO2)}(\omega_Q^{(i)})} [1 - \Pi^{(G)}(\omega_Q^{(i)}) - \Pi^{(S)}(\omega_Q^{(i)})] , \quad (22)$$

and similarly for $\Phi^{(TO2)}(\omega_Q^{(i)})$. Once more, it has been verified numerically that these definitions satisfy the additional normalization conditions:

$$\sum_{i=1}^{4} \Phi^{(TO1)}(\omega_Q^{(i)}) = 1 , \quad \sum_{i=1}^{4} \Phi^{(TO2)}(\omega_Q^{(i)}) = 1 , \quad (23)$$

and, for each mode $i$:

$$\Pi^{(G)}(\omega_Q^{(i)}) + \Pi^{(S)}(\omega_Q^{(i)}) + \Phi^{(TO1)}(\omega_Q^{(i)}) + \Phi^{(TO2)}(\omega_Q^{(i)}) = 1 . \quad (24)$$

At sufficiently short wavelengths plasmons cease to be proper excitations. In our context this may happen when the gate-plasma-like solution $\omega_Q^{(i_g)}$ (where usually $i_g = 1$ at large enough $N_g$) enters the single-particle continuum in the gate, the substrate-plasma-like solution enters the single-particle continuum in the substrate, or both. In order to account for Landau damping, albeit approximately, we proceed as follows. Whenever the substrate-plasmon-like excitation $\omega_Q^{(i_s)}$ (where, usually, $i_s = 4$) enters the single-particle continuum of the 2DEG evaluated in the extreme quantum limit (*i.e.*, $\omega_Q^{(i_s)} \le [(\hbar Q)/(2m_t)](Q+2K_F)$, where $K_F = (\pi n_s)^{1/2}$, $m_t = 0.19 m_0$ being the transverse effective mass), we consider only the three solutions $\omega_Q^{(-s,i)}$ ($i = 1,3$) given above. These represent the three coupled gate-plasmon/insulator-TO-modes which exist when the substrate plasma is absent. The plasmon/phonon content and scattering strength for these modes are obtained in a way completely analogous to the one discussed so far. Similarly, when the frequency of the gate-plasmon-like excitation enters the single-particle continuum of gate (that is, $\omega_Q^{(i_g)} \le (\hbar Q)/(2m_g)(Q + 2k_F)$, where $k_F$ is the zero-temperature Fermi wave vector of the electron gas in the gate, $k_F = (\pi^2 N_g/2)^{1/3}$, and the index $i_g$ takes a value of 1 or 2, depending on electron density in the gate, frequency of the high-energy TO-mode, $\omega_{TO2}$, and dielectric constants of the material considered), we consider only the three solutions $\omega_Q^{(-g,i)}$ ($i = 1,3$) representing the three coupled substrate-plasmon /insulator-TO-modes which exist when the gate plasma does

not respond. In this case only phonon-like scattering with these modes is considered. Equation (33) describes the surface-phonon scattering field, setting $\epsilon_{gate}(\omega) = \epsilon_{Si}^{\infty}$ in $\epsilon_{TOT,high}^{(TOi)}(\omega)$ and $\epsilon_{TOT,low}^{(TOi)}(\omega)$ to reflect the absence of the gate plasma.

Finally, when both the gate- and the substrate-plasmons-like dispersions are within their respective Landau-damping regions, we consider only the two phonon-like modes of frequencies $\omega_Q^{(SOi)}$ ($i$ = 1,2), whose associated scattering field is given by Eq. (33) with $\epsilon_{gate}(\omega) = \epsilon_{substrate}(Q,\omega) = \epsilon_{Si}^{\infty}$ employed into $\epsilon_{TOT,high}^{(TOi)}(\omega)$ and $\epsilon_{TOT,low}^{(TOi)}(\omega)$.

### B. Scattering strength

The amplitude $a_{Q,\omega}$ of the field, Eq. (7), can be determined using the semiclassical approach originally proposed by Stern and Ferrel[12] which we also followed in Ref. 7 and described in a simple case in Appendix A of Ref. 8. We first consider the time-averaged total (electrostatic, including self-energy) energy, $< W_Q^{(i)} >$, associated with the field $\phi_Q^{(i)}(\mathbf{R},z,t)$ caused by the excitation of mode $i$ oscillating at the frequency $\omega_Q^{(i)}$. (The bra-kets $< ... >$ denote time average). Let us write the electrostatic potential at a given wavelength as:

$$\phi_Q^{(i)}(\mathbf{R},z,t) \ = \ \phi_{Q,\omega_Q^{(i)}}^{(i)}(z) \ \cos(\mathbf{Q}\cdot\mathbf{R} - \omega_Q^{(i)}t) \ . \tag{25}$$

Since phonons and plasmons in the harmonic and linear-response approximations, respectively, are represented as harmonic oscillations, the time-averaged total energy associated with these excitations is simply twice the time-averaged potential energy, $< U_Q^{(i)} >$. This, in turn, is the electrostatic (self)energy of the interface polarization charge density $\rho_Q^{(i)}(\mathbf{R},z,t)$ in the presence of the potential $\phi_Q^{(i)}(\mathbf{R},z,t)$ caused by the interface charge itself. We may express this potential energy in two alternative equivalent ways: From the expression (7) for the potential, the density of the polarization charge associated with mode $i$ is localized at the two interfaces and can be obtained from the Poisson equation $\rho_Q^{(i)}(\mathbf{R},z,t) = -\nabla \cdot [\epsilon(\omega_Q^{(i)};z)\nabla\phi_Q^{(i)}(\mathbf{R},z,t)]$ (where the $z$-dependence in $\epsilon(\omega_Q^{(i)};z)$ reflects the fact the we must use the appropriate dielectric functions across the interfaces):

$$\begin{aligned}\rho_Q^{(i)}(\mathbf{R},z,t) \ = \ \{\delta(z) \ [ \ \epsilon_{gate}(\omega_Q^{(i)}) \ a_{Q,\omega_Q^{(i)}} \ + \ \epsilon_{insulator}(\omega_Q^{(i)}) \ (b_{Q,\omega_Q^{(i)}} - c_{Q,\omega_Q^{(i)}}) \ ] \\ + \ \delta(z-t) \ [ \ \epsilon_{insulator}(\omega_Q^{(i)})(c_{Q,\omega_Q^{(i)}}e^{Qt} - b_{Q,\omega_Q^{(i)}}e^{-Qt}) \\ + \ \epsilon_{substrate}(Q,\omega_Q^{(i)}) \ d_{Q,\omega_Q^{(i)}}e^{-Qt} \ ] \ \} \ Q \ \cos(\mathbf{Q}\cdot\mathbf{R} - \omega_Q^{(i)}t) \ ,\end{aligned} \tag{26}$$

having introduced the new functions $\epsilon_{gate}(\omega)$, $\epsilon_{insulator}(\omega)$, and $\epsilon_{substrate}(Q,\omega)$ which must be chosen in a way consistent with the component of the polarization charge $\rho_Q^{(i)}(\mathbf{R},z,t)$ we are considering, as discussed below. Therefore, for the energy $< W_Q^{(i)} >$ we can write:

$$< W_Q^{(i)} > = \ 2 \ < U_Q^{(i)} > = \ \frac{2}{\Omega}\left\langle \int_\Omega d\mathbf{R} \ \int_{-\infty}^{\infty} \ dz \ \phi_Q^{(i)}(\mathbf{R},z,t) \ \rho_Q^{(i)}(\mathbf{R},z,t)\right\rangle \ , \tag{27}$$

where $\Omega$ is a normalization area. Alternatively, using Green's identity and accounting for the discontinuity of the electric and displacement fields across the interfaces, we can

express $< W_Q^{(i)} >$ in terms of the electrostatic energy of the field $\mathbf{E}_Q^{(i)} = -\nabla \phi_Q^{(i)}$:

$$< W_Q^{(i)} > = \frac{2}{\Omega} \left\langle \int_\Omega d\mathbf{R} \int_{-\infty}^{\infty} dz \ \epsilon(\omega_Q^{(i)}; z) \ |\mathbf{E}_Q^{(i)}(\mathbf{R}, z, t)|^2 \right\rangle . \tag{28}$$

From Eqns. (8-10) and either using Eq. (27) or performing the integrals in Eq. (28) using Eq. (7), we obtain:

$$< W_Q^{(i)} > = \ Q \ \epsilon_{TOT}(Q, \omega_Q^{(i)}) \left[ \frac{\epsilon_{ox}(\omega_Q^{(i)}) - \epsilon_g(\omega_Q^{(i)})}{\epsilon_{ox}(\omega_Q^{(i)}) + \epsilon_s(Q, \omega_Q^{(i)})} \right]^2 a^2_{Q,\omega_Q^{(i)}} \ e^{-2Qt} . \tag{29}$$

Here the 'total' effective dielectric function of the substrate coupled to the gate and the insulating layer has been defined as:

$$\begin{aligned} \epsilon_{TOT}(Q, \omega) \ &= \ \epsilon_{gate}(\omega) \left[ \frac{\epsilon_{ox}(\omega) + \epsilon_s(Q, \omega)}{\epsilon_{ox}(\omega) - \epsilon_g(\omega)} \right]^2 e^{2Qt} \\ &+ \ \epsilon_{insulator}(\omega) \left\{ \left[ \frac{\epsilon_{ox}(\omega) + \epsilon_s(Q, \omega)}{2\epsilon_{ox}(\omega)} \right]^2 (e^{2Qt} - 1) \ + \ \left[ \frac{\epsilon_{ox}(\omega) - \epsilon_s(Q, \omega)}{2\epsilon_{ox}(\omega)} \right]^2 (1 - e^{-2Qt}) \right\} \\ &+ \ \epsilon_{substrate}(Q, \omega) \ , \end{aligned} \tag{30}$$

having made repeated use of the relations (6) to reach one of the many possible equivalent algebraic forms. The semiclassical nature of the argument enters the final step of setting the quantity $< W_Q^{(i)} >$ equal to the zero-point energy, $\hbar\omega_Q^{(i)}/2$, of the quantized excitation. This finally determines the 'normalization constant', $a_{Q,\omega_Q^{(i)}}$, and thus the amplitude of the scattering field in the substrate ($z \geq t$):

$$\phi^{(i)}_{Q,\omega_Q^{(i)}} \ = \ \left[ \frac{\hbar\omega_Q^{(i)}}{2 \ Q \ \epsilon_{TOT}(Q, \omega_Q^{(i)})} \right]^{1/2} \ e^{-Q(z-t)} \ , \tag{31}$$

up to the appropriate Bose factors of the excitations, ${n_Q^{(i)}}^{1/2}$ and $(1 + n_Q^{(i)})^{1/2}$, which multiply the scattering potential for absorption and emission processes, respectively.

The choice of the dielectric functions $\epsilon_{gate}(\omega)$, $\epsilon_{insulator}(\omega)$, and $\epsilon_{substrate}(Q, \omega)$, which appear in the expression for $\epsilon_{TOT}(Q, \omega)$, is a crucial element of our discussion. Whenever we are interested in determining the potential energy due to a particular type of response of the system (ionic or electronic), we cannot include this response into these dielectric functions. For example, by setting $\epsilon_{gate}(\omega) = \epsilon_g(\omega)$, $\epsilon_{insulator}(\omega) = \epsilon_{ox}(\omega)$, and $\epsilon_{substrate}(Q, \omega) = \epsilon_s(Q, \omega)$, we effectively lump the entire dielectric response, ionic and electronic, into the dielectric functions, and we expect that the potential energy of 'whatever response is left' (none, in this case) in the field and charge, $\phi_Q$ and $\rho_Q$, should vanish. Indeed when so doing, the resulting $\epsilon_{TOT}(Q, \omega)$ vanishes for $\omega = \omega_Q^{(i)}$, the equation $\epsilon_{TOT}(Q, \omega) = 0$ being equivalent to the secular equation (6). So, when taking $\epsilon_{gate}(\omega) = \epsilon_{Si}^{\infty}$, $\epsilon_{substrate}(Q, \omega) = \epsilon_{Si}^{\infty}$, and $\epsilon_{insulator}(\omega) = \epsilon_{ox}^0$ we consider only the plasmon contribution to the polarization charges. Indeed, the response of the insulator lattice is removed from the electrostatic field by being lumped into the insulator permittivity when setting $\epsilon_{insulator}(\omega) = \epsilon_{ox}^0$, while the electronic response is removed from the

dielectric functions of the gate and substrate, and is included directly into the amplitude of the electrostatic field and polarization charge, $\phi_Q$ and $\rho_Q$. In this case Eq. (31) represents the amplitude of the field induced by plasma excitations. Thus, defining as $\epsilon_{TOT}^{(PL)}(Q,\omega_Q^{(i)})$ the total plasma dielectric function so obtained, scattering between electrons in the substrate and gate plasmons is described by the effective scattering field:

$$\phi^{(i,g,PL)}_{Q,\omega_Q^{(i)}}(z) \;=\; \left[\frac{\hbar\omega_Q^{(i)}}{2\;Q\;\epsilon_{TOT}^{(PL)}(Q,\omega_Q^{(i)})}\;\Pi^{(G)}(\omega_Q^{(i)})\right]^{1/2}\; e^{-Q(z-t)}\;. \tag{32}$$

Scattering with the field induced by the polarization charges of the insulator lattice (*i.e.*, with the optical phonons in the insulator) can be evaluated in a way essentially identical to the approach followed by Kittel[13] to evaluate the Fröhlich coupling in bulk polar materials. The only difference between Kittel's and our approach consists in following Stern and Ferrel[12] in evaluating the ground-state energy semiclassically, rather than from second-order perturbation theory. In order to isolate the contribution of each phonon independently and consider only the lattice polarization, the squared, time-averaged amplitude of the scattering field is computed by lumping the electronic response into the dielectric functions of the gate and substrate, while letting one phonon (say, phonon 2 to fix the ideas) respond, but first by 'freezing' the other mode (TO1) and then by considering its full response. The difference between the two squared amplitudes so obtained constitutes the effect of the ionic polarization charge associated solely with the optical mode 1. To be explicit, in our case the amplitude of the field (31) when only phonon 2 responds is obtained by setting $\epsilon_{gate}(\omega)=\epsilon_g(\omega)$ (response of the gate plasmons lumped into the gate dielectric function), $\epsilon_{substrate}(Q,\omega)=\epsilon_s(Q,\omega)$ (response of the substrate plasmons lumped into the dielectric function of the inversion layer), and setting $\epsilon_{insulator}(\omega)=\epsilon_{ox}^{\infty}(\omega_{LO2}^2-\omega^2)/(\omega_{TO2}^2-\omega^2)$ (phonon 2 responds at the frequency $\omega$, while phonon 1 does not respond). Let $\epsilon_{TOT,high}^{(TO1)}$ be the resulting effective dielectric function. On the contrary, when phonon 1 is allowed to respond fully, we have $\epsilon_{insulator}(\omega)=\epsilon_{ox}^{\infty}[(\omega_{LO2}^2-\omega^2)/(\omega_{TO2}^2-\omega^2)](\omega_{LO1}/\omega_{TO1})^2$ (which reduces to $\epsilon_{ox}^0$ in the simpler case of insulators exhibiting only one TO-mode), the full response of phonon 1 now being accounted for by the term $(\omega_{LO1}/\omega_{TO1})^2$. Let $\epsilon_{TOT,low}^{(TO1)}$ denote the resulting dielectric function. Thus, the interaction between electrons in the inversion layer and the TO1-phonon-content of the mode $i$ will be described by the scattering field:

$$\phi^{(i,PH1)}_{Q,\omega_Q^{(i)}}(z) \;=\; \left\{\frac{\hbar\omega_Q^{(i)}}{2Q}\left[\frac{1}{\epsilon_{TOT,high}^{(TO1)}(Q,\omega_Q^{(i)})}-\frac{1}{\epsilon_{TOT,low}^{(TO1)}(Q,\omega_Q^{(i)})}\right]\;\Phi^{(TO1)}(\omega_Q^{(i)})\right\}^{1/2}\; e^{-Q(z-t)}\;. \tag{33}$$

The scattering strength with phonon mode 2 can be trivially obtained by swapping the indices 1 and 2 in the discussion above.

### C. Discussion

We summarize graphically the results of this section by showing in Figs. 2 and 3 the significant properties of the interface modes for the Si/$SiO_2$/Si and the Si/$ZrO_2$/Si systems, respectively, as a function of the in-plane wave vector $Q$. These two MOS systems are the extreme cases of a low-$\kappa$ ($SiO_2$) and a high-$\kappa$ ($ZrO_2$) material, the Si/$SiO_2$/Si system exhibiting some of the stiffest modes, the Si/$ZrO_2$/Si some of the softest optical modes. The curves in the figures have been obtained using electron

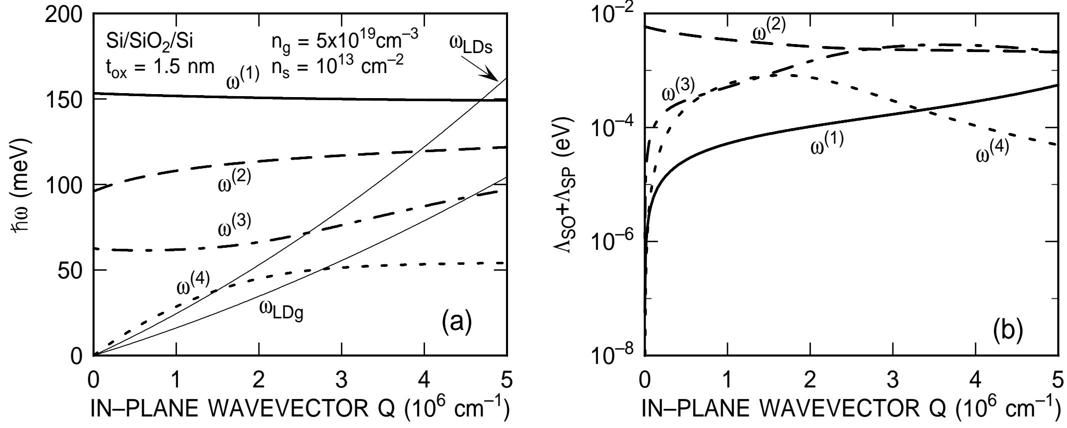


**Fig.** 2: Calculated dispersion (a) and total scattering strength (b) for the insulator-optical-phonon/substrate-and-gate-plasmons interface modes for the Si/SiO$_2$/Si system. In (a), the curves labeled by $\omega_{LDs}$ and $\omega_{LDg}$ identify the boundary of the substrate and gate Landau-damping regions, respectively. Modes 5 and 6 have been ignored.

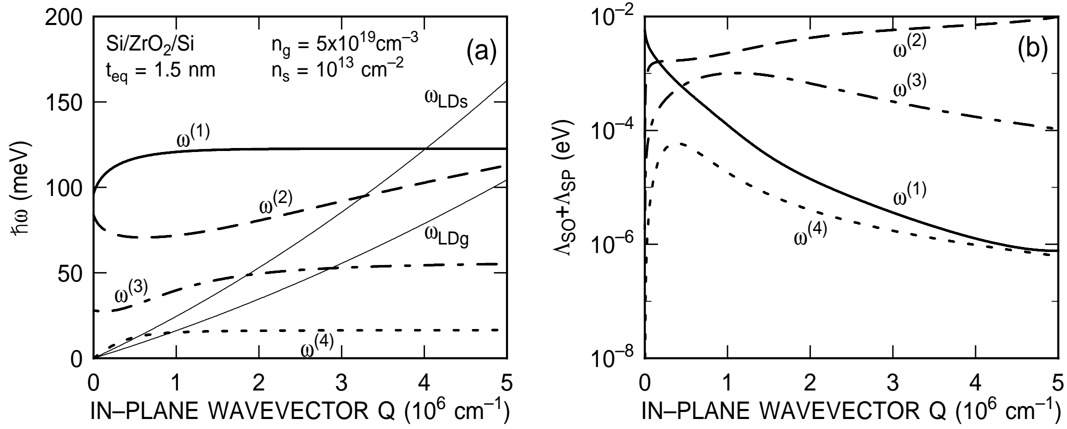


**Fig.** 3: As in Fig. 2, but for the Si/ZrO$_2$/Si system. Note that the two highest-energy modes are plasmon-like.

concentrations in the gate and in the Si substrate and an 'equivalent' insulator thickness, $t_{eq}$, (defined as $t\epsilon_{ox}^0/\epsilon_{SiO_2}^0$), which are representative of typical situations. The subband model employed has been described in Sec. II of Ref. 7: We have employed an anisotropic, non-parabolic band-structure, used a triangular-well approximation for the potential in the inversion layer, and embraced the long-wavelength approximation for the dielectric function discussed above, also ignoring intersubband-plasmons.

In Figs. 2 and 3 we show in (a) the dispersion of the modes and in (b) the total scattering strength for each mode. The scattering strength with the phonon-like component of each mode $i$, $\Lambda_{SO}^{(i)}(Q)$, has been defined, according to Eq. (33), by summing the scattering strength of both TO-modes $\alpha$:

$$\Lambda_{SO}^{(i)}(Q) = \sum_{\alpha=1}^{2} \Lambda_{SO,\alpha}^{(i)}(Q)$$

$$= \epsilon_0 \sum_{\alpha=1}^{2} \left| \frac{\hbar\omega_Q^{(i)}}{2} \left[ \frac{1}{\epsilon_{TOT,high}^{(TO\alpha)}(Q,\omega_Q^{(i)})} - \frac{1}{\epsilon_{TOT,low}^{(TO\alpha)}(Q,\omega_Q^{(i)})} \right] \Phi^{(TO1)}(\omega_Q^{(i)}) \right| , \quad (34)$$

and similarly for the scattering strength for the gate-plasmon content of mode $i$, $\Lambda_{SP}^{(i)}(Q)$, defined, according to Eq. (32), as:

$$\Lambda_{SP}^{(i)}(Q) \ = \ \epsilon_0 \ \left| \frac{\hbar\omega_Q^{(i)}}{2\ \epsilon_{TOT}^{(PL)}(Q,\omega_Q^{(i)})} \ \Pi^{(G)}(\omega_Q^{(i)}) \right| \ . \tag{35}$$

(In both Eqns. (34) and (35) we have included a factor $\epsilon_0$ to give the scattering strengths an 'intuitive' dimension of energy.) Note that, comparing Eq. (33) with Eq. (34) and Eq. (32) with Eq. (35), the (squared) scattering amplitude will be modulated by a factor $Q^{-1}$ – which is compensated by the density-of-states factor $Q$ while integrating over final scattering states. The scattering field will also exhibit the exponential decay $\exp[-Q(z-t)]$ into the substrate, away from the substrate/insulator interface.

Landau damping has been ignored in these figures. However, the two curves labeled $\omega_{LDg}$ and $\omega_{LDs}$ identify the region of strong damping of the gate and substrate plasma, respectively. As explained above, Landau damping is approximately accounted for by ignoring the substrate plasma for values of $Q$ such that $\omega^{(4)} \geq \omega_{LDs}$ (in both figures) and by ignoring the response of the gate electrons whenever $\omega^{(2)} \geq \omega_{LDg}$ (in Fig. 2) or $\omega^{(1)} \geq \omega_{LDg}$ (in Fig. 3).

In Fig. 2(a), the mode labeled $\omega^{(1)}$ appears clearly to be mostly a phonon-like mode, originating from the high-frequency $SiO_2$ TO-mode at about 0.135 eV. The mode $\omega^{(2)}$ is mainly a gate-plasmon mode, its coupling to the high-frequency phonon mode increasing at shorter wavelengths. The second, low-energy $SiO_2$ TO-mode at about 0.06 eV is strongly coupled to the substrate plasmons. Indeed, the modes labeled $\omega^{(3)}$ and $\omega^{(4)}$ result from this strong coupling: The former is mostly phonon-like at small $Q$, but it quickly becomes mainly a substrate-plasma mode as $Q$ grows, while the mode $\omega^{(4)}$ shows the opposite behavior.

Figure 3 conveys essentially the same information, but it shows how the stiffest mode, labeled $\omega^{(1)}$, is now mainly gate-plasmon-like, mode $\omega^{(2)}$ is mainly phonon-like at small $Q$, substrate-plasmon-like at shorter wavelength. The mode labeled $\omega^{(3)}$ is mainly phonon-like, but its phonon content switches from the low-energy (small $Q$) to the high-energy (large $Q$) insulator phonon mode, crossing the substrate-plasma mode at intermediate wavelength. The mode labeled $\omega^{(4)}$ starts as substrate-plasma-like at low $Q$, but it becomes almost completely phonon-like at larger $Q$.

Although not shown in the figures, the $SiO_2$-system ($\omega^{(2)}$) shows a larger gate-plasmon scattering strength than for the $ZrO_2$-system ($\omega^{(1)}$). As explained before[7], this is simply due to the closer proximity of the gate in the $SiO_2$-system. Conversely, looking at the scattering strength of the $\omega^{(2)}$-mode, for example, at the largest values of $Q$ in the undamped region, the $ZrO_2$-system exhibits a stronger scattering strength with phonon-like modes. Finally phonon-like scattering with modes $\omega^{(3)}$ (in Fig. 2) and $\omega^{(2)}$ (in Fig. 3) is significantly enhanced by the phonon-plasmon coupling. This effect results from the anti-screening properties of the electron gas(es). Whenever the frequency of an excitation is larger than the frequency of the electron plasma, the coupling strength with the excitation is enhanced, while Landau damping gains strength. Indeed this effect is significant well within the region in which we must account for Landau damping. In our case the situation is noticeably complicated by the presence of two plasmas (the gate and the substrate) and by two optical phonons. As we shall see below discussing the effective electron mobility, each of the phonon-like excitations may be screened by

one plasma and anti-screened by the other.

## III. EFFECTIVE MOBILITY OF THE 2D ELECTRON GAS

### A. The model

The calculation of the effective electron mobility in the inversion layer of the MOS systems considered here has been performed using the approximations and models described in detail in Sec. III of Ref. 7. We have employed Eq. (63) of that reference, using the total relaxation time computed by adding relaxation rates due to electron scattering with intravalley, intra- and inter-subband acoustic phonon using an anisotropic deformation potential (Eq. (86) of Ref. 7), scattering with intervalley phonons as described in Sec. III D of that reference, and considering scattering with the coupled plasmon/insulator-phonon interface modes employing Eq. (77) of Ref. 7, but substituting the 'effective' field amplitude $|\mathcal{A}_Q|^2$ with the scattering strengths $\Lambda^{(i)}_{SO,\alpha}(Q)/Q$ and $\Lambda^{(i)}_{SP}(Q)/Q$ given by Eqns. (34) and (35) above. The Si inversion layer has been modeled using the triangular well approximation, employing a number of subbands sufficient to account correctly for absorption processes by thermal electrons.

The complexity and computer requirements of the numerical procedure limit the maximum number of subbands (and so on the minimum electron density) which we could consider. Even so, some 'numerical noise' is evident in our results. The dispersion of the interfacial modes has been obtained by solving the secular equation (6) for a set of tabulated values $Q_i$ and storing its roots in look-up tables. In general there will be four of them in the undamped region of low $Q$, three or only two as Landau damping enters the picture at larger values of $Q$. We also tabulate, for each $Q$ and branch $i$, the amplitude of the scattering fields and the group velocity of the modes, required to evaluate the Jacobian factor $g$ (in the notation of Ref. 7). A linear interpolation of these functions of the magnitude of the momentum-transfer $Q$ has been performed during the numerical integration of the SO-limited relaxation time.

The electron concentration, $N_g$, entering the evaluation of the gate plasma has been estimated by first integrating numerically the Poisson equation in the gate for a given electron concentration, $n_s$, in the inversion layer of the Si substrate. We have then either employed the electron concentration at the insulator/gate interface, or, instead, the average quantity

$$< N_g(Q) > = \frac{\int_{z_{max}}^{0^-} N(z)\ e^{Qz}\ dz}{\int_{z_{max}}^{0^-}\ e^{Qz}\ dz}\ . \tag{36}$$

This expression has a heuristic justification. The potential associated with the interface excitations has the form given by Eq. (7), exhibiting an exponential decay $e^{Qz}$ for $z \leq 0$. Therefore, the 'effective' average electron density seen in the gate by an interface excitation will approach the gate donor density, $N_{Dg}$, at long wavelength and $N(z = 0^-)$ at short wavelength. Equation (36) empirically captures this behavior. Note that this $Q$-dependent average must be employed to compute the dispersion of the interface modes, since it appears via $\omega_{p,g}$, and so via $\epsilon_g(\omega)$, in the secular equation (6).

Finally, scattering with interface roughness has been included using Matthiessen's rule and adding to the calculated mobility $\mu_{PH,SO,SP}$ – including scattering with Si phonons (PH), coupled surface-optical (SO), and interface plasmons (SP) modes - the

contribution of a surface-limited mobility, $\mu_{SR}$ of the form $\mu_{SR} = \mu_0(10^{13}/n_s)^2$, with $n_s$ measured in cm$^{-2}$. The constant $\mu_0$ has been determined by fitting the resulting 'total' mobility $\mu_{tot} = [1/\mu_{PH,SO,SP} + 1/\mu_{SR}]^{-1}$ calculated for thick (5nm) $SiO_2$-systems at $n_s = 10^{13}$ cm$^{-2}$ to the experimental value in lightly-doped substrates of about 308 cm$^2$/Vs (see Ref. 15). The resulting value was $\mu_0 = 1.473 \times 10^3$ cm$^2$/Vs when using $N_g = N(z = 0^-)$, and $\mu_0 = 1.167 \times 10^3$ cm$^2$/Vs when using $N_g = < N_g(Q) >$. Converting the latter value to commonly used expressions, it implies a surface-roughness-limited mobility about a factor of 2 larger than what we obtained in the past[6] (using Monte Carlo simulations, and also used in Fig. 1, which assumed the values $\Lambda = 1.3$ nm and $\Delta = 0.48$ nm for the Ando's parameters[14]), and within 10% of a typical empirical fit[16] to the effective electron mobility.

### B. Insulator parameters

We have considered MOS systems with 6 different insulators: $SiO_2$, $Al_2O_3$, AlN, $ZrO_2$, $HfO_2$, and $ZrSiO_4$. These materials cover a range of parameters (dielectric constants, phonon energies, etc.) wide enough to give an idea of the qualitative bahavior of the electron mobility as a function of the physical properties of the insulator.

In order to select the parameters required to evaluate the electron/SO-modes scattering strength, it is convenient to rewrite Eq. (11) in the following more general form accounting for $N_{TO}$ TO-modes:

$$\epsilon_{ox}(\omega) \;=\; \epsilon_{ox}^{\infty} \;+\; \epsilon_0 \sum_{\alpha=1}^{N_{TO}} \frac{f_\alpha \, \omega_{TO,\alpha}^2}{\omega_{TO,\alpha}^2 - \omega^2} \;. \tag{37}$$

We can relate this expression to its alternative form, Eq. (11), by rewriting the oscillator strength $f_\alpha$ of the TO-mode $\alpha$ in terms of the 'intermediate' dielectric constants $\epsilon^{(\alpha)} \approx \epsilon_{ox}(\omega_\alpha)$, where $\omega_{\alpha-1} \leq \omega_{TO,\alpha} < \omega_\alpha$ for $\omega_\alpha$ ordered so that $\omega_{\alpha-1} < \omega_\alpha$:

$$f_\alpha \;=\; \frac{\epsilon^{(\alpha-1)} \;-\; \epsilon^{(\alpha)}}{\epsilon_0} \;. \tag{38}$$

Here $\epsilon^{(\alpha=0)} \;=\; \epsilon_{ox}^0$ and $\epsilon^{(\alpha=N_{TO})} \;=\; \epsilon_{ox}^{\infty}$. For a single TO-mode and, approximately, for TO-modes widely separated energetically, the Lyddane-Sachs-Teller (LST) relation provides the LO/TO splitting:

$$\omega_{LO,\alpha}^2 \;\approx\; \frac{\epsilon^{(\alpha-1)}}{\epsilon^{(\alpha)}} \, \omega_{TO,\alpha}^2 \;. \tag{39}$$

For materials exhibiting two or more TO-modes at nearby frequencies, the energy of the LO-modes must be determined by the generalized LST-relation $\epsilon_{ox}(\omega) \;=\; 0$, such as Eq. (14) valid in the case of two TO-phonons. In order to determine completely the frequency dependence of $\epsilon_{ox}(\omega)$ in the model-form (37), for each bulk mode $\alpha$ we need knowledge of two of the quantities $\omega_{TO,\alpha}$, $\omega_{LO,\alpha}$, and $\epsilon^{(\alpha)}$ (or, equivalently, $f_\alpha$). Experimentally, Infrared (IR) absorption experiments can provide mainly information on $\omega_{TO,\alpha}$, while Raman and electron tunneling-spectroscopy[17] can also provide direct information about the LO-frequency, $\omega_{LO,\alpha}$. The relative amplitude of each peak in the IR spectra can be correlated with the oscillator strength $f_\alpha$. In addition, one could rely on theoretical calculations. Unfortunately, things are more complicated. Our ultimate

**Table** 1: Parameters used to compute the electron-phonon coupling in polar insulators. The frequency of the optical phonons and/or the dielectric functions $\epsilon^0$, $\epsilon^i$, and $\epsilon^\infty$ are taken from the literature, when available, and the unavailable data are obtained using the Lyddane-Sachs-Teller relation. When more than two modes are present, only the two strongest modes (based on the magnitude of the LO-TO energy splittings) have been considered. When anisotropic quantities are given – such as in Refs. 24 and 36 for the energies of $E_T$ and $A_{2T}$ (bc tetragonal) or $E_u$ and $A_{2u}$ (hexagonal) modes propagating in directions perpendicular and parallel to the crystal $c$-axis, respectively, and also for the elements of the dielectric tensor – a simple average has been taken. The Fröhlich coupling constants for each mode are also indicated. Note the large coupling constants for the low-energy modes in $ZrO_2$ and $HfO_2$, which are indeed the materials yielding the lowest mobility.

| Material<br>Quantity (units) | $SiO_2^{(a)}$ | $Al_2O_3^{(b)}$ | $AlN^{(c)}$ | $ZrO_2^{(d-f)}$ | $HfO_2^{(f,g)}$ | $ZrSiO_4^{(h)}$ |
|---|---|---|---|---|---|---|
| $\epsilon^0_{ox}$ ($\epsilon_0$) | 3.90 | 12.53 | 9.14 | 24.0$^{(i)}$ | 22.00 | 11.75 |
| $\epsilon^i_{ox}$ ($\epsilon_0$) | 3.05 | 7.27 | 7.35 | 7.75 | 6.58 | 9.73 |
| $\epsilon^\infty_{ox}$ ($\epsilon_0$) | 2.50 | 3.20 | 4.80 | 4.00 | 5.03 | 4.20 |
| $\omega_{TO1}$ (meV) | 55.60 | 48.18 | 81.40 | 16.67 | 12.40 | 38.62 |
| $\omega_{TO2}$ (meV) | 138.10 | 71.41 | 88.55 | 57.70 | 48.35 | 116.00 |
| $\alpha_1$ | 0.0248 | 0.0788 | 0.0248 | 0.2504 | 0.3102 | 0.0322 |
| $\alpha_2$ | 0.0113 | 0.0814 | 0.0423 | 0.0779 | 0.0362 | 0.2942 |

($a$) Refs. 4 and 24 and references therein.
($b$) Ref. 25.
($c$) Ref. 18.
($d$) Ref. 28.
($e$) Ref. 29.
($f$) Ref. 27.
($g$) Ref. 33.
($h$) Ref. 36 and references therein.
($i$) Ref. 31.

goal is the calculation of the electron mobility, possibly comparing our results with experimental data. However, as thin-insulator MOS structures are typically manufactured with processes which must be compatible with the current Si technology, The structure and composition of the grown or deposited insulator can often be inferred only indirectly. The dielectric response of any given material may depend on its morphology: For example, AlN exhibits different properties in its wurtzite and zinc-blende structure[18]. It can also depend on its closeness to the ideal chemical composition: Incompletely oxidized $Al_2O_3$, for example, shows additional modes, possibly related to unoxidized Al ions[19]. Undesired, but so far unavoidable, 'native' interfacial layers ($SiO_2$ when dealing with oxides, $Si_3N_4$ when dealing with nitrides) can mask the response of the 'pure' dielectric under study, as discussed in Sec. IV. Finally, the information available in the literature is incomplete, occasionally inconsistent. Here we shall rely on both experimental data and theoretical results, and we shall compare this input with with Fourier transform infrared (FTIR) spectra we have obtained, and attempt to obtain a consistent picture. Some of these have already been reported, including experimental details[20]. Additional spectra are shown in Fig. 4. Table 1 summarizes the values we have employed.

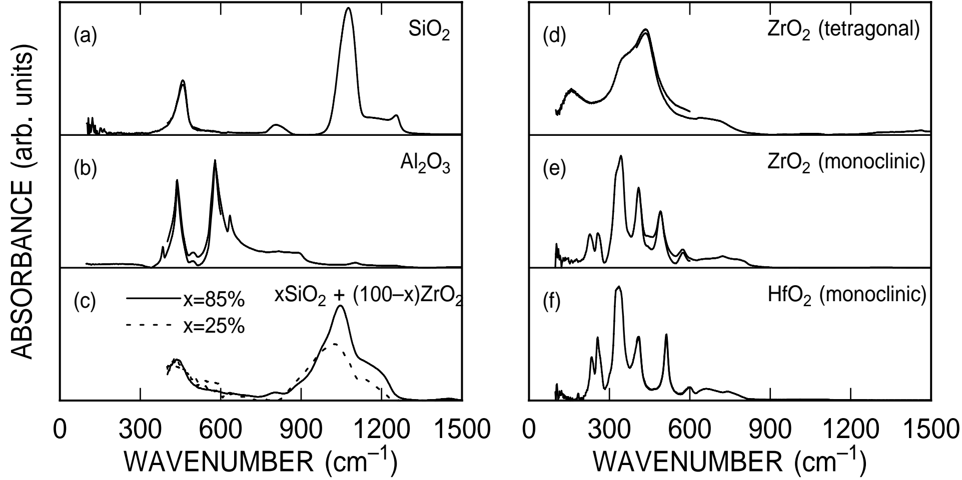


**Fig.** 4: FTIR spectra for some of the insulators considered. In all spectra (except for $x$SiO$_2$+(100-$x$)ZrO$_2$ with $x$=85% in the bottom panel) two curves are shown, one in the far-IR range of 50 to 600 cm$^{-1}$ and one in the mid-IR range of 400 to 4000 cm$^{-1}$. In the bottom frame ('nominally' ZrSiO$_4$ obtained from chemical-solution deposition of $x$SiO$_2$+(100-$x$)ZrO$_2$) spectra for $x$=85% and $x$=25% are shown, to illustrate the decay of the SiO$_2$-mode at about 1080 cm$^{-1}$ with decreasing $x$.

In the table we also show the dimensionless coupling constant

$$\alpha_i = \frac{e^2}{4\pi\hbar} \left(\frac{m_t}{2\hbar\omega_{SOi}}\right)^{1/2} \left(\frac{1}{\epsilon_{Si}^{\infty} + \epsilon_{ox}^{\infty}} - \frac{1}{\epsilon_{Si}^{\infty} + \epsilon_{ox}^{0}}\right) , \tag{40}$$

for each of the two modes $i$, which corresponds to the dimensionless Fröhlich coupling constant usually defined in bulk materials. These coupling constants have been obtained using for the energy of the SO-phonons the approximate expressions given by Eq. (2), with the appropriate optical, static, and 'intermediate' dielectric constants. Note how well these values correlate with the mobility shown in Fig. 1. In particular, the high values of the coupling constants relative to the low-energy modes in HfO$_2$ and ZrO$_2$ hint very directly at the importance of remote scattering with SO-modes in MOS systems using these materials.

The FTIR spectra of SiO$_2$ were obtained from thermally grown SiO$_2$. The $\alpha$-Al$_2$O$_3$ FTIR spectra were obtained from a chemical-solution-deposited film annealed at 1200 C for 60 minutes in oxygen. The FTIR spectra of tetragonal and monoclinic ZrO$_2$ were obtained from chemical-solution-deposited films annealed at 500 C and 900 C, respectively. The FTIR spectra of $x$SiO$_2$ +(100-$x$)ZrO$_2$ with $x$= 85% and 25% were obtained from a chemical-solution-deposited film annealed at 700 C. Additional details regarding deposition, phase formation, and FTIR analysis of the ZrO$_2$, HfO$_2$ and $x$SiO$_2$ +(100-$x$)ZrO$_2$ films can be found in the literature[20]. The monoclinic HfO$_2$ spectra were obtained from a film chemical-vapor-deposited at 700 C.

*SiO$_2$*. The SiO$_2$ FTIR spectrum shown in Fig. 4 exhibits two strong peaks at 1076 and 461 cm$^{-1}$, corresponding to TO-modes at 133.4 and 57.2 meV, associated with an asymmetric stretching of the SiO$_4$ unit and a bending of the Si-O-Si bond, respectively. We neglect a weak third mode at 806 cm$^{-1}$ ($\approx$ 100 meV), due to a symmetric stretching mode of the Si-O-Si bond. The 'shoulders' at 1255 and 532 cm$^{-1}$ are related to the corresponding LO modes. These values are in good agreement with the experimental energies reported by Hess and Vogl[4] - from Refs. 21- 23. Also the

LO/TO splittings are consistent with the oscillator strengths reported in the literature, but those derived from the areas under the FTIR peaks appear to give a stronger high-energy mode, the strength of the mode 1076 $\mathrm{cm}^{-1}$ being about 5 times stronger than the strength of the low-energy phonon. We have decided to use the most common values for the oscillator strengths reported in the literature. Indeed, recent calculations of the Raman-active intensities in $\alpha$-quartz, based on a first-principle density functional approach, give a variety of modes.[24] Averaging the two strongest transverse modes over symmetry directions (the $A_{2T}$ and $E_T$ modes at the $\Gamma$ point) gives two modes at about 1100 and 450-480 $\mathrm{cm}^{-1}$. A similar average over the longitudinal modes ( $A_{2L}$ and $E_L$) provides the LO/TO energetic splitting and, via the LST relation Eq. (39) and Eq. (38), a ratio of 3:4 for the oscillator strengths of the modes.

*$Al_2O_3$*. Two peaks are clearly visible in the FTIR spectrum, at 579 and 437 $\mathrm{cm}^{-1}$ for a film deposited at 600 C and annealed in oxygen at 1200 C for 60 minutes to ensure complete oxidation. The areas under the peaks yield a ratio 56:44 for their respective oscillator strengths. High-resolution energy loss spectroscopy in thin $Al_2O_3$ films provides two sets of modes, in the plane of the film and off-plane[25]. The in-plane TO-modes (at 578 and 390 $\mathrm{cm}^{-1}$) are in fair agreement with our FTIR results. Chen and co-workers[19] see a variety of modes as a function of annealing conditions of the thin films, typically grouped into three LO bands around 400-430, 600-655, and 850-895 $\mathrm{cm}^{-1}$. The low-energy band is attributed to excess (unoxidized) Al. The remaining two bands are in satisfactory agreement with the TO energies and oscillator strengths which can be derived from the FTIR spectrum and Ref. 25. The selection reported in Table 1 can be viewed as a satisfactory compromise.

*AlN*. For AlN we employ the theoretical results by Ruiz and co-workers[18] (an *ab initio* Hartree-Fock study of the hexagonal (wurtzite) phase of AlN) and by Gorczyca *et al.*[26] (a muffin-tin analysis of both the wurtzite and zinc-blende phases). In the hexagonal phase two almost degenerate TO modes (at around 660 and 715 $\mathrm{cm}^{-1}$, with oscillator strengths in a 59:41 ratio) originate from a single cubic TO mode at about 650 $\mathrm{cm}^{-1}$, as a result of the doubling of the available optical modes moving from the cubic to the hexagonal structure. For the wurtzite phase, the modes reported in Table 1 have been obtained by averaging the modes over the various allowed symmetries. The particular structure selected (wurtzite or zinc-blende) is largely immaterial as far as electron scattering is concerned, since the total oscillator strength carried by the almost-degenerate modes in the hexagonal phase coresponds approximately to the oscillator strength of the the single mode in the cubic phase. Finally, we have neglected a weak low-energy mode at 250 $\mathrm{cm}^{-1}$ seen in Raman spectra, reported in Refs. 18 and 26.

*$ZrO_2$*. Desgreniers and Lagarec[27] have published Raman spectra for polycrystalline (cotunnite phase) $HfO_2$ and $ZrO_2$. For the latter insulator, they have observed two TO modes at wavenumbers of about 390 (an oscillation of the Zr-O bond) and 100 $\mathrm{cm}^{-1}$, with the corresponding LO modes at about 430 and 170 $\mathrm{cm}^{-1}$. Raman spectra by Morell and co-workers[28] for Y- and Ca-stabilized $ZrO_2$ give two LO modes at 620 and 160 $\mathrm{cm}^{-1}$, the former mode possibly influenced by the dopants. Lattice-dynamics calculations for cubic and tetragonal lattices[29] give three transverse modes at wavenumbers 164 ($E_u$), 339, and 467 ($A_{2u}$) $\mathrm{cm}^{-1}$, with corresponding longitudinal frequencies at 232, 354, and 650 $\mathrm{cm}^{-1}$. These values, in rough agreement with the dispersions calculated by Mirgorodsky *et al.*[30] for cubic and tetragonal $ZrO_2$, show that the 339(TO)/354(LO)-

cm$^{-1}$ $A_{2u}$-mode is quite weak. In Fig. 4 we show FTIR spectra we have obtained for both tetragonal and monoclinic $ZrO_2$. The former exhibits a weak peak at 161 cm$^{-1}$, a weak shoulder at about 300 cm$^{-1}$, signature of the weak 339 cm$^{-1}$ mode reported in Refs. 29 and 30, and a stronger structure around 439 cm$^{-1}$. These are in good agreement with both the experimental[27] and the theoretical[29,30] frequencies we have just discussed. The spectrum relative to tetragonal $ZrO_2$ is quite similar, while showing sharper peaks. Therefore, we have employed the LO-energies reported in Ref. 29, but have lowered the TO-frequency of the low-energy mode to account for the higher static dielectric constant ($\sim 24\ \epsilon_0$) observed in thin films[31]. Note that in FTIR spectra oscillations at wavenumbers below about 100 cm$^{-1}$ remain elusive, as impurities (dopants) in the Si substrate render it opaque to the IR radiation.

*$HfO_2$*. The dominant high-frequency mode seen in the Raman spectra of Ref. 27 (TO at 395 cm$^{-1}$ with corresponding LO at 450 cm$^{-1}$) – a vibration of the Hf-O bond – is also seen in the FTIR spectrum of this material in the monoclinic phase, as a double peak around 337-409 cm$^{-1}$. It corresponds to one of the modes of the monoclinic structure also reported in Ref. 32. The low-frequency mode seen in the spectrum of Ref. 27 (TO at 115 cm$^{-1}$, LO at 210 cm$^{-1}$), despite its strength is not easily visible in IR spectroscopy, as explained above. Thus, we have embraced essentially unaltered the results of Ref. 27, using the values for the refractive index from Refs. 34 and 35, and ignoring the weaker modes at 235 and 256 cm$^{-1}$ seen in the spectrum of Fig. 4.

*$ZrSiO_4$*. FTIR spectra of chemical-solution deposited $x$SiO$_2$+(100-$x$)ZrO$_2$ (with $x$ in percent) films, such as those shown in Fig. 4 or in Ref. 20, usually show two TO bands (a strong one at 430-460 cm$^{-1}$, a weaker one around 810-930 cm$^{-1}$). A strong signal around 1080 cm$^{-1}$ can be attributed to residual 'unconverted' $SiO_2$, since, as shown by the dashed line in the bottom spectrum of Fig. 4, its intensity decreases with decreasing $x$. Averaging over the frequencies of the $A_{2u}$ and $E_u$ modes calculated for bc tetragonal $ZrSiO_4$ by Rignanese and co-workers[36], the two strongest modes appear to be at approximately 310 and 940 cm$^{-1}$ (with corresponding LO wavenumbers at 410 and 1060 cm$^{-1}$). The relative oscillator strengths are approximately in the ratio 73:27. The low-energy mode can be assigned to an oscillation of the Zr-O bond, the high-energy mode to a vibration of the Zr-O-Si bond. Using the dielectric constants reported in Ref. 36 and the index of refraction from Ref. 37, we obtain the values shown in Table 1.

### C. Results

Before presenting the results of our calculations including the full dielectric response of the gate and substrate electron plasmas and their coupling with the optical modes of the insulating layer, it is interesting to revisit Fig. 1. The results shown in this figure illustrate the effect of the polar field of the optical modes of the insulators on the mobility of the electrons in the inversion layer, as determined by the parameters discussed in the previous section and by the simple Wang-Mahan scattering strength given by Eq. (1). Let's recall that in these calculations screening effects of the electrons in the inversion layer are ignored, as well as screening by the (infinitely far) gate.

$SiO_2$ (dots, solid line) is moderately affected by the presence of the SO modes, as a comparison with the curve calculated by neglecting them (open circles, dashed line) reveals. As stated in our introductory section, the stiffness of the Si-O bond results in a high-frequency LO-mode which couples poorly with thermal electrons, and a mode

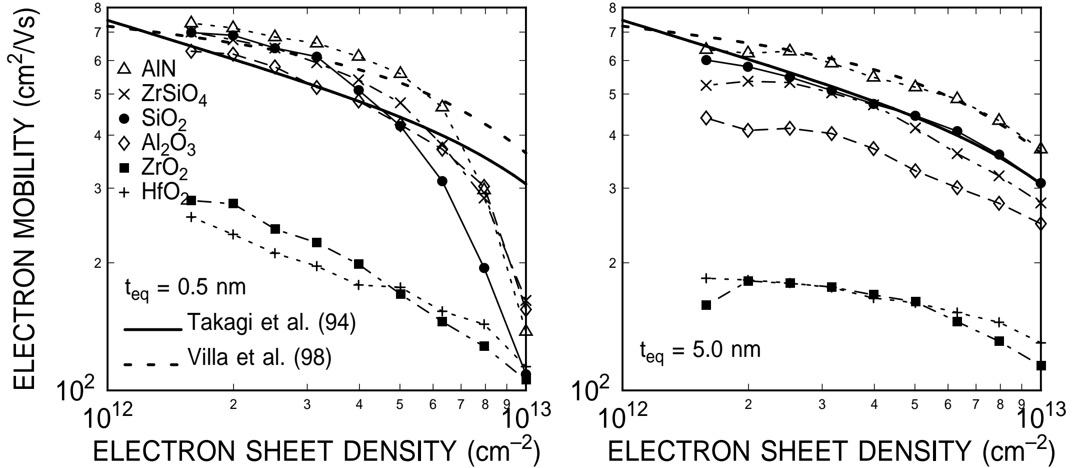


**Fig.** 5: Calculated effective electron mobility in the inversion layer of MOS systems with various insulators for the '$SiO_2$-equivalent' thicknesses of 0.5 (left) and 5.0 nm (right). The Kubo-Greenwood expression for the mobility has been used by employing an anisotropic momentum relaxation time accounting for scattering with bulk Si phonons, gate/insulator interface plasmons (SP), and surface-optical (SO) insulator phonon. The effect of scattering with interface roughness at the substrate/insulator interface has been included by fitting the experimental mobility for the $SiO_2$-based system at an electron density of $10^{13}$ cm$^{-2}$ and using Matthiessen's rule. The plasma response of the depleted poly-Si gate has been assumed to be given by the electron concentration at the gate/insulator interface determined by a numerical solution of the Poisson equation. In both frames the 'universal mobility curve' by Takagi *et al.*[15] (thick solid line) and an empirical fit from Ref. 16 (thick dashed line) show the range of experimental value. All data refer to systems with negligible scattering with dopants in the substrate or charges in the insulator.

of lower frequency with a small coupling constant, Eq. (1). Thus, SO-modes have a very small effect, of about 5%, on the electron mobility. AlN has a somewhat larger dielectric constant (9.14) and in its wurtzite phase exhibits two almost degenerate modes at energies still larger than the thermal temperature. As for $SiO_2$, the electron mobility is only moderately affected by the presence of these phonons. But as soon as we consider materials with soft metal-oxygen bonds, the dielectric constant raises, and so does also the Wang-Mahan coupling. In addition, modes of lower energy – usually caused by oscillations of the oxygen ion in metal-O bonds – emerge and couple very effectively with thermal electrons. The insulators with the highest $\kappa$ ($ZrO_2$ and $HfO_2$) are negatively affected by the presence of low-energy modes and by the larger electron/SO-phonon coupling constant, exhibiting the lowest mobility over the entire range of electron sheet densities. The dependence of the mobility on $n_s$ is almost completely dominated by scattering with the SO-modes and by the electronic form-factor (overlap intergral) entering the expression for the relaxation rate associated with this process (see Eq. (79) of Ref. 7). $Al_2O_3$ and $ZrSiO_4$ are intermediate materials, both as far as their mobility as well as their dielectric constant are concerned.

In Figs. 5 and 6 we now show the effective mobility accounting for the plasmon/TO-phonon coupling, and for the screening (or anti-screening) effects of the gate and substrate plasma. We show results relative to two $SiO_2$-equivalent insulator thicknesses: infinitely-thick insulators, and 0.5 nm. In Fig. 5 we have employed the gate/insulator surface electron concentration to determine the bulk plasma frequency of the gate, as determined by the solution of the Poisson equaton. In Fig. 6, instead, we have employed the $Q$-dependent average, $< N_g(Q) >$, given by Eq. (36) above. We see a few major differences between Fig. 1 on the one side, and Figs. 5 and 6 on the other: Screening

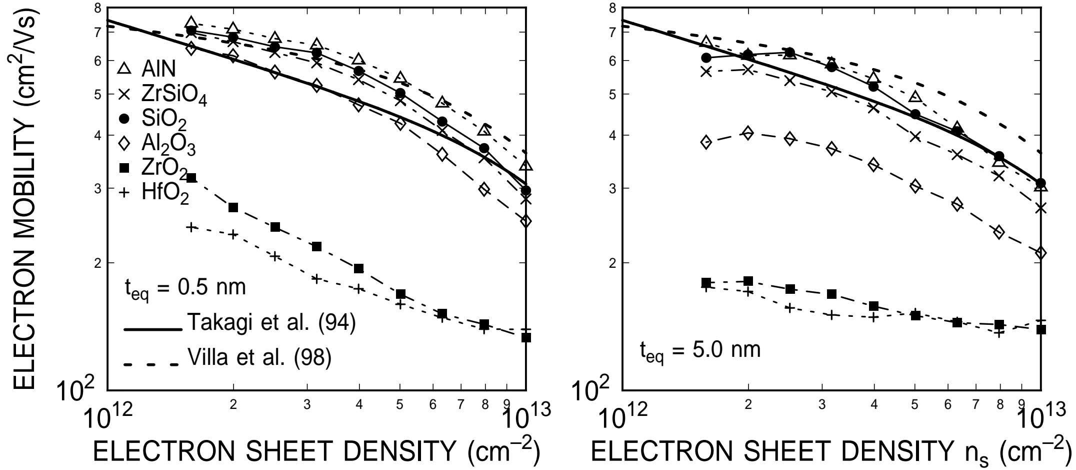


**Fig.** 6: As in Fig. 5, but with the plasma response of the depleted poly-Si gate now computed using a wave vector dependent average electron concentration in the depletion layer of the gate.

of the electron-SO scattering by the substrate electrons themselves results in a higher mobility for $ZrO_2$ and $HfO_2$ at large $n_s$: In these materials the mobility is dominated by SO-scattering, the relevant SO-modes have relatively low energy, so their influence can be effectively screened by 2D-plasmons of higher frequency. At lower sheet densities, however, the frequency of the interface excitations becomes larger than the plasma frequency of the 2DEG in the substrate, and anti-screening takes effect, boosting the scattering rate and lowering the mobility with respect to the unscreend value shown in Fig. 1. At the smaller $t_{eq}$, however, another interesting effect emerges: Screening by the electrons in the gate. For sufficiently small electron sheet densities in the substrate, $n_s \leq 5 \times 10^{12}$ cm$^{-2}$, $SiO_2$, AlN, $Al_2O_3$, and $ZrSiO_4$ exhibit mobilities approaching the value limited only by scattering with Si phonons. Even the mobilities of $ZrO_2$ and $HfO_2$ improve at these small densities, as a result of the competition between gate screening and substrate anti-screening.

The difference between the results shown in Fig. 5 and those shown in Fig. 6 is not qualitative, but only quantitative. Since the choice of a $Q$-dependent average $< N_g(Q) >$ results in a larger gate plasma frequency over most of the interesting range of values for $Q$, scattering with gate plasmons and the reduction of the SO-frequency is less pronounced in the dispersions used in Fig. 6. This results in large effective mobilities at large values of $n_s$.

In Figs. 7 and 8 we show the dependence on the thickness of the insulator of the various components of the mobility. Note in Fig. 7 that the SP-limited mobility is quite large even for $SiO_2$ and at the smallest $t_{eq}$ investigated, because both of Landau damping and of the large gate-plasma frequency at the small electron density in the inversion layer (and so larger electron density in the gate) assumed in the figure ($n_s = 1.54 \times 10^{12}$ cm$^{-2}$).[7] Note also the screening effect of the gate plasma on the SO-limited mobility at small $t_{eq}$. On the contrary, at the larger electron density employed in in Fig. 8 ($n_s = 10^{13}$ cm$^{-1}$) we see all of the effects which our previous discussions, here and in Ref. 7, had anticipated: Scattering with (gate) surface plasmons is negligible (*i.e.*, small enough not to contribute significantly to the total mobility) in all materials, except obviously $SiO_2$. On the contrary, this 'advantage' of the high-$\kappa$ materials is unfortunately more than compensated by a much stronger scattering with the TO-components of the interface excitation. The SO-limited mobility decreases at small $t_{eq}$ – as also evident in Fig. 5

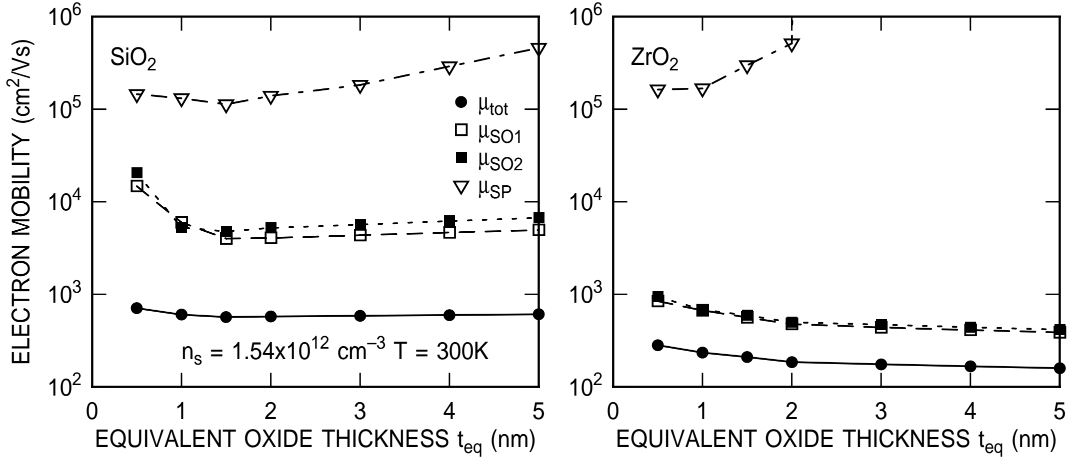


**Fig.** 7: Calculated components of the total mobility ($\mu_{tot}$) at an electron sheet density in the substrate of $1.54 \times 10^{12}$ cm$^{-2}$ as function of the '$SiO_2$-equivalent' thickness $t_{eq}$ for the $SiO_2$- (left) and $ZrO_2$-based MOS structures (right). The curves labeled $\mu_{SO1}$ and $\mu_{SO2}$ refer to the components of the mobility limited by scattering with the TO1 and TO2 phonon-like components of the interface modes. The curve labeled $\mu_{SP}$ has been obtained from the total mobility and the SO-limited mobilities using Matthiessen's rule. The total mobility accounts for scattering with bulk Si phonons, SO- and SP-limited processes, but it does not account for scattering with interface roughness.

– because of the anti-screening effect of a strongly depleted gate: When using the gate/insulator interface electron concentration, the strongly depleted gate will exhibit a lower plasma frequency, and so it will be unable to screen the SO-component of the scattering field, actually anti-screening it. Finally, in Fig. 9 we show the dependence of the SO-limited electron mobility on the static dielectric constant of the insulator. We have chosen a relatively small value for the electron concentration, in order to minimize the effect of scattering with surface roughness and with the gate-plasmon component of the interface excitations. Thus, the SO-limited component of the mobility is the major correction to the Si-phonon-limited component in the absense of Coulomb scattering with dopants and insulator charges. Note how the mobility decreases monotonically as $\kappa$ increases, thanks to the softer oxygen bonds. AlN is indeed the single exception, thanks to the higher energy of the nitrogen-related optical phonons.

## IV. EFFECT OF A SILICON DIOXIDE INTERFACIAL LAYER

In this final section we discuss the effect caused by the presence of a thin layer of $SiO_2$ between the Si substrate and the high-$\kappa$ dielectric on the electron mobility in the Si inversion layer. In particular, we have in mind the *beneficial* effect of the interfacial layer in MOS systems based on materials (such as $HfO_2$ or $ZrO_2$) exhibiting a large ionic polarizability, so that removing the high-$\kappa$ layer farther away from the Si substrate should reduce the strong interaction with the SO-modes of the high-$\kappa$ dielectric. Therefore, the formation of a thin $SiO_2$ layer may be not only hard to avoid during the growth/deposition/annealing of the high-$\kappa$ insulator, but also desirable. To formulate more precisely our expectations, note that the length-scale relevant for the calculation of the electron mobility is the Fermi wavelength of the 2DEG, $\lambda_F \sim K_F^{-1} \sim n_s^{-1/2}$. Since the scattering potential decays with increasing distance $z$ from the high-$\kappa$ insulator as $\exp(-Qz)$, the effects of an $SiO_2$ interfacial layer of thickness $t_{ox}$ will be of 1. turning on the interaction with $SiO_2$ SO-modes, which we have seen

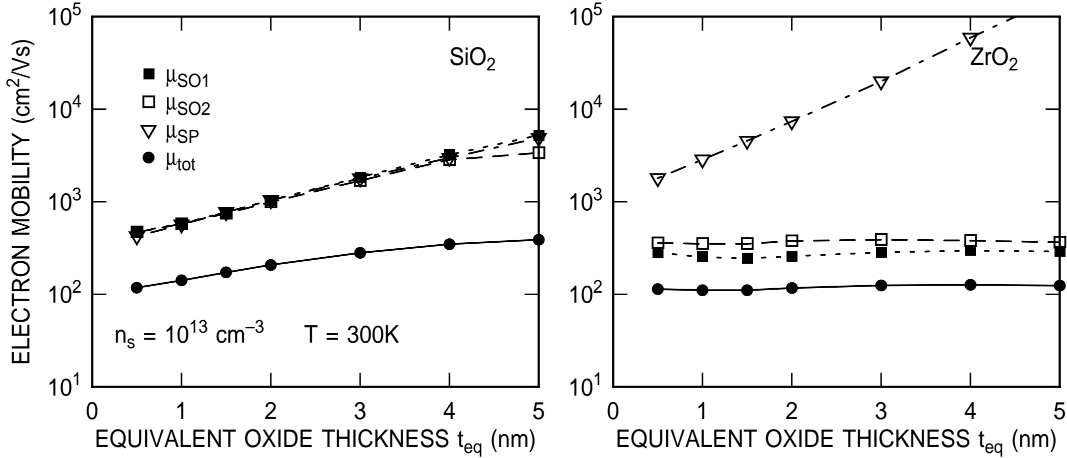


**Fig.** 8: As in Fig. 7, but at an electron density in the substrate of $10^{13}$ cm$^{-2}$.

is quite small, and 2. reducing the scattering strength of the high-$\kappa$ SO-modes by a factor $\sim \exp(-2K_F t_{ox})$. At small electron sheet densities $n_s$, the small value of the Fermi wave vector means that unreasonably thick oxides are required in order to boost the electron mobility. Not so at large $n_s$ (and so at large $K_F$), in which case even a 0.5-1.0 nm-thick $SiO_2$ layer can have a significant beneficial effect.

The analysis of the coupled plasmon-phonon modes of the full Si-gate/high-$\kappa$/$SiO_2$/Si system is quite cumbersome. Following a trivial generalization of the procedure described in Sec. II.A, the secular equation – whose solutions yield the dispersion of the modes – takes the form of a 16-th degree algebraic equation in $\omega^2$. Even using the long-wavelength approximations for the dielectric functions, the problem is extermely cumbersome, the 16 positive solutions representing the dispersion of the 16 coupled modes resulting from 2 TO-like modes in each insulating film, and 12 surface modes (at large $Q$ identifiable as groups of four modes mainly localized at each one of the three interfaces).

Here our aim is just to investigate qualitatively the effects caused by the interfacial layer. Thus, we reduce the complexity of the problem by making the following approximations.

1. A comparison between Fig. 1 and Figs. 5 or 6 shows that the 'infinitely-thick insulator limit' captures the most important qualitative (and even quantitative) aspects of the problem. Thus, it seems appropriate to consider the simpler infinitely-thick-high-$\kappa$/$SiO_2$/Si system and ignore electronic screening effects. Thus, the dispersion of the modes is given by the solutions of the secular equation

$$\epsilon_{ox}(\omega)^2 \ + \ \epsilon_{ox}(\omega)[\epsilon_\kappa(\omega) + \epsilon_{Si}^\infty] \ \mathrm{cotanh}(Qt_{ox}) \ + \ \epsilon_{ox}(\omega)\epsilon_{Si}^\infty \ = \ 0 \ . \qquad (41)$$

   This is exactly Eq. (6) with the role of the gate now played by the high-$\kappa$ dielectric and with $\epsilon_s(Q,\omega)$ replaced by $\epsilon_{Si}^\infty$.

2. Low-energy SO modes are most important in determining the electron mobility. Thus, we approximate the response of the two insulators considering only their low-energy TO phonons and employ dielectric functions of the form:

$$\epsilon_{ox}(\omega) \ = \ \epsilon_{ox}^i \ \frac{\Omega_{LO}^2 - \omega^2}{\Omega_{TO}^2 - \omega^2} \ , \qquad \epsilon_\kappa(\omega) \ = \ \epsilon_\kappa^i \ \frac{\omega_{LO}^2 - \omega^2}{\omega_{TO}^2 - \omega^2} \qquad (42)$$

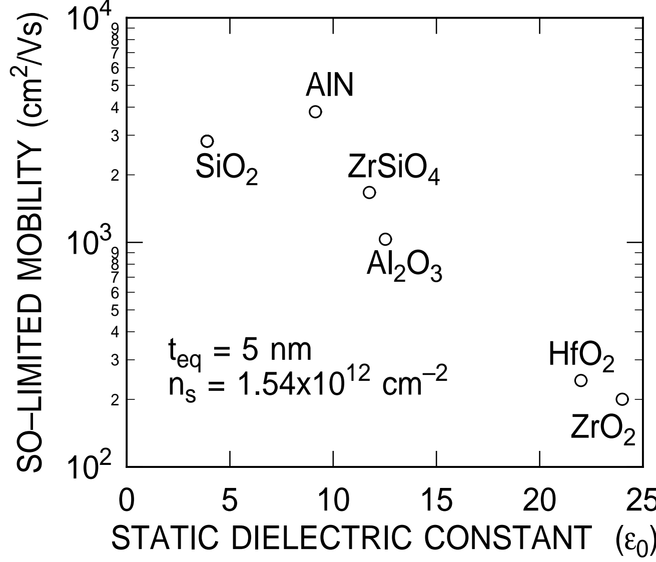


**Fig.** 9: Calculated SO-limited component of the electron mobility in the inversion layer of MOS systems with various insulators at an electron density of $1.54 \times 10^{12}$ cm$^{-2}$ as a function of the static dielectric constant of the insulator.

where $\Omega_{LO} = (\epsilon^0_{ox}/\epsilon^i_{ox})^{1/2}\Omega_{TO}$ and $\omega_{LO} = (\epsilon^0_\kappa/\epsilon^i_\kappa)^{1/2}\omega_{TO}$ are the longitudinal frequencies of the low-energy optical modes of the $SiO_2$ and high-$\kappa$ layers, respectively.

3. Since we are most interested in understanding how 'low-mobility' materials behave in the presence of the interfacial oxide layer, and since these materials usually exhibit very soft optical modes, we typically have $\omega_{TO} << \Omega_{TO}$, as seen in Table 1 for $HfO_2$ and $ZrO_2$. Therefore, the $SiO_2$ and high-$\kappa$ modes become largely decoupled. In the fully-decoupled limit, excellent approximations of the three solutions of Eq. (41) are given by:

$$\omega_Q^{(\kappa)} \approx \left( \frac{\epsilon^0_\kappa + \Delta_Q^{(\kappa)}}{\epsilon^i_\kappa + \Delta_Q^{(\kappa)}} \right)^{1/2} \omega_{TO} \ , \tag{43}$$

where $\Delta_Q^{(\kappa)} = \epsilon^0_{ox}[\epsilon^0_{ox} + \epsilon^\infty_{Si}\text{cotanh}(Qt_{ox})]/[\epsilon^\infty_{Si} + \epsilon^0_{ox}\text{cotanh}(Qt_{ox})]$, and

$$\omega_Q^{(\pm)} \approx \left( \frac{\epsilon^0_{ox} + \Delta_Q^{(\pm)}}{\epsilon^i_{ox} + \Delta_Q^{(\pm)}} \right)^{1/2} \Omega_{TO} \ , \tag{44}$$

where $2\Delta_Q^{(\pm)} = (\epsilon^i_\kappa + \epsilon^\infty_{Si})\text{cotanh}(Qt_{ox}) \pm \{[(\epsilon^i_\kappa + \epsilon^\infty_{Si})\text{cotanh}(Qt_{ox})]^2 - 4\epsilon^\infty_{Si}\epsilon^i_\kappa\}^{1/2}$. The solution $\omega_Q^{(\kappa)}$ represents the SO-mode associated with the TO phonon of the high-$\kappa$ film. For small $Qt_{ox}$ the solution $\omega_Q^{(+)}$ approaches $\Omega_{TO}$, thus being essentially a bulk $SiO_2$ TO-mode, while in the limit of large $Qt_{ox}$ it approaches the frequency of the $SiO_2$ mode at the 'far' high-$\kappa$/$SiO_2$ interface. In either limit, this mode couples only weakly with the electrons in the inversion layer and – while retaining it – could safely be neglected, similarly to the modes labeled $\omega_Q^{(5)}$ and $\omega_Q^{(6)}$ in Sec. II.A.

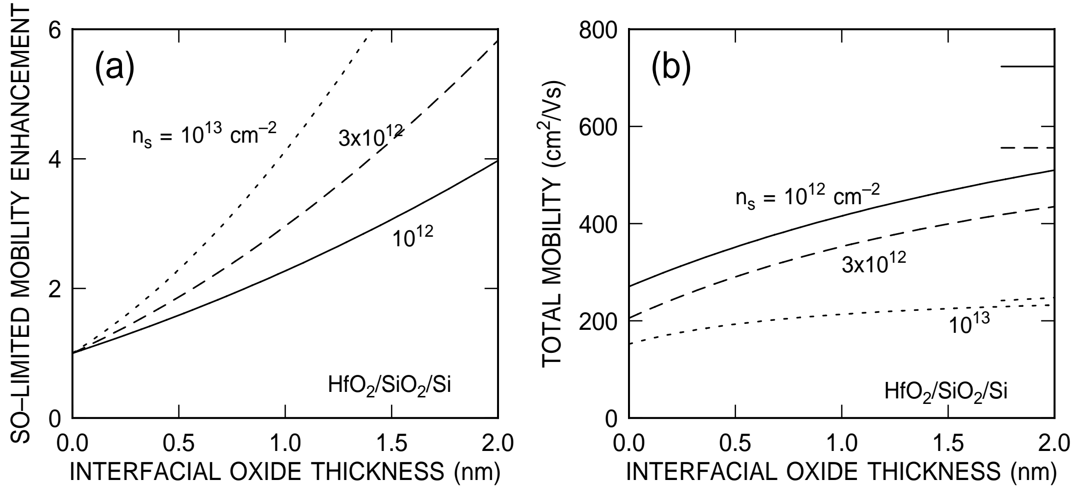


**Fig.** 10: (a) Calculated enhancement of the SO-limited mobility in the inversion layer of a $HfO_2/SiO_2/Si$ system as a function of thickness of the interfacial $SiO_2$ layer for the three indicated values of the electron concentration in the inversion layer. An infinitely thick $HfO_2$ layer and only the low-energy TO-modes in the insulators have been consider ed. For a given thickness of the interfacial oxide, the enhancement is larger at large electron densities, since the length-scale is set by the Fermi wavelength of the two-dimensional electron gas. (b) Calculated total electron mobility (including scattering with Si phonons and interfacial roughness), as in (a). The horizontal lines at the far right are the asymptotic limits of infinite oxide thickness (*i.e.*, the mobility for the 'pure' $Si/SiO_2$ interface). As in (a), in order to approach the mobility at the $Si/SiO_2$ interface, a thicker $SiO_2$ interfacial layer is required at lower electron sheet density.

Finally, the solution $\omega_Q^{(-)}$ is the SO-mode at the Si/SiO2 interface associated with the $SiO_2$ TO-mode. All modes, $\omega_Q^{(\kappa)}$ and $\omega_Q^{(\pm)}$, exhibit a very weak dependence on $Q$. We shall ignore their dispersion and employ their short-wavelength limits, $\omega_Q^{(\kappa)} \approx \omega_{TO}[(\epsilon_\kappa^0 + \epsilon_{Si}^\infty)/(\epsilon_\kappa^i + \epsilon_{Si}^\infty)]^{1/2}$, $\omega_Q^{(+)} \approx \Omega_{TO}[(\epsilon_{ox}^0 + \epsilon_\kappa^\infty)/(\epsilon_{ox}^i + \epsilon_\kappa^\infty)]^{1/2}$, and $\omega_Q^{(-)} \approx \Omega_{TO}[(\epsilon_{ox}^0 + \epsilon_{Si}^\infty)/(\epsilon_{ox}^i + \epsilon_{Si}^\infty)]^{1/2}$. The scattering strength associated with the high-$\kappa$ mode can be obtained as in Sec. II.B:

$$\Lambda^{(\kappa)}(Q) = \frac{\hbar\omega_Q^{(\kappa)}}{2}\left[\frac{1}{\epsilon_{TOT}^{\kappa,hi}(Q)} - \frac{1}{\epsilon_{TOT}^{\kappa,lo}(Q)}\right] , \qquad (45)$$

where

$$\epsilon_{TOT}^{\kappa,hi/lo}(Q) = \epsilon_\kappa^{i/0}\left[\frac{\epsilon_{ox}(\omega)+\epsilon_{Si}^\infty}{\epsilon_{ox}(\omega)-\epsilon_\kappa(\omega)}\right]^2 e^{2Qt_{ox}}$$
$$+ \epsilon_{ox}(\omega)\left\{\left[\frac{\epsilon_{ox}(\omega)+\epsilon_{Si}^\infty}{2\epsilon_{ox}(\omega)}\right]^2 (e^{2Qt_{ox}}-1) + \left[\frac{\epsilon_{ox}(\omega)-\epsilon_{Si}^\infty}{2\epsilon_{ox}(\omega)}\right]^2 (1-e^{-2Qt_{ox}})\right\} + \epsilon_{Si}^\infty, \qquad (46)$$

where the last expression is evaluated for $\omega = \omega_Q^{(\kappa)}$. Similarly, for the scattering strength of the modes $\omega_Q^{(\pm)}$ we get:

$$\Lambda^{(\pm)}(Q) = \frac{\hbar\omega_Q^{(\pm)}}{2}\left[\frac{1}{\epsilon_{TOT}^{ox,hi}(Q)} - \frac{1}{\epsilon_{TOT}^{ox,lo}(Q)}\right] , \qquad (47)$$

where

$$\epsilon_{TOT}^{ox,hi/lo}(Q) \;=\; \epsilon_{\kappa}(\omega) \left[ \frac{\epsilon_{ox}(\omega) + \epsilon_{Si}^{\infty}}{\epsilon_{ox}(\omega) - \epsilon_{\kappa}(\omega)} \right]^2 \; e^{2Qt_{ox}}$$

$$+ \; \epsilon_{ox}^{i/0} \left\{ \left[ \frac{\epsilon_{ox}(\omega) + \epsilon_{Si}^{\infty}}{2\epsilon_{ox}(\omega)} \right]^2 (e^{2Qt_{ox}} - 1) \; + \; \left[ \frac{\epsilon_{ox}(\omega) - \epsilon_{Si}^{\infty}}{2\epsilon_{ox}(\omega)} \right]^2 (1 - e^{-2Qt_{ox}}) \right\} \; + \; \epsilon_{Si}^{\infty}, \tag{48}$$

where $\epsilon_{\kappa}(\omega)$ and $\epsilon_{ox}(\omega)$ are evaluated at $\omega = \omega_Q^{(\pm)}$. Note that, as expected, $\Lambda^{(\kappa)}(Q) \sim e^{-2Qt_{ox}}$ while $\Lambda^{(\pm)}(Q) \to 0$ as $Qt_{ox} \to 0$.

4. Finally, we consider only one subband in the inversion layer. Therefore, the electron mobility can be obtained using Eqns. (68) and (85) of Ref. 7 (the latter equation unfortunately being mistyped in that reference: the factor $b^6 e^{-2Qt_{ox}}$ in the integrand should be replaced by unity), by substituting $|\mathcal{A}_Q|^2$ with $[\Lambda^{(\kappa)}(Q) + \Lambda^{(+)}(Q) + \Lambda^{(-)}(Q)]/Q$ in Eq. (85).

We show in Fig. 10 our results for the $HfO_2/SiO_2/Si$ system, similar results having been obtained also for the $ZrO_2/SiO_2/Si$ system. The top frame shows the enhancement of the SO-limited mobility resulting from the presence of the $SiO_2$ interfacial layer, *i.e.*, the ratio between the SO-limited mobility calculated for the $HfO_2/SiO_2/Si$ system with an $SiO_2$ layer of thickness $t_{ox}$, and the mobility calculated using the same approximations for the 'pure' infinitely-thick-$HfO_2$/Si system. As expected, a 1.0 nm-thick interfacial $SiO_2$ layer boosts the SO-limited mobility by a factor of more than 4 at the largest electron density considered ($10^{13}$ cm$^{-2}$), but an $SiO_2$ layer as thick as 2.0 nm is required to obtain the same enhancement at the lowest density ($10^{12}$ cm$^{-2}$). The bottom frame illustrates the dependence of the overall mobility (accounting also for scattering with Si phonons and surface roughness, included empirically using Matthiessen's rule). The horizontal lines at the far right indicated the asymptotic limit of an infinitely thick $SiO_2$ layer. Once more, at the largest density the mobility of the 'pure' infinitely-thick-$SiO_2$/Si system is recovered quickly even for thin interfacial layer. Not so at the lowest density: Even in the presence of a 1.0 nm-thick interfacial oxide layer, we remain almost a factor of 2 below the 'desired' $SiO_2$/Si limit.

## V. DISCUSSION AND CONCLUSIONS

The mobilities shown in Figs. 5 and 6 show a clear trend, emphasized in Fig. 9. It appears that the price one must pay for a higher $\kappa$ is a reduced electron mobility. Among the materials we have investigated, metal-oxides appear to be the worst, because of the soft modes caused by the oscillation of the oxygen ions, while AlN and, to some extent $ZrSiO_4$, show significant promise, albeit with the caveats we shall mention below.

Several sources of uncertainty affect the quantitative accuracy of our results: First and foremost is the choice of parameters for the insulators. This concerns both the overall quality of the parameters listed in Table 1 for 'ideal' materials, as well as their applicability to 'real' insulators, almost invariably of a 'non-ideal' composition and structure. This has been already discussed above and will be emphasized again in the following paragraph. Second, the difference between the results shown in Fig. (5) and those shown in Fig. (6) clearly points at the importance of knowing accurately the electron density in the depletion layer of the gate. Again, this source of uncertainty affects not only the 'ideal' calculations we have performed, but also the 'real world'

complications we should expect: The poly-crystalline structure of the Si gate, for example, will undoubtely result in an electron concentration exibiting inhomogeneities not only in the $z$-direction, but also on the plane of the interface. Dopant segregation at grain boundaries is another possible cause of inhomogeneities. Nevertheless, our results stress at least qualititatively (but, hopefully, also quantitatively) the major role played by the gate both in screening the electron-SO interaction, as well as in triggering the gate/substrate Coulomb drag studied in Ref. 7. In particular, we should note that the use of metal gates should be beneficial in both cases, by inducing a more complete screening of the surface optical modes and by reducing the plasmon-mediated (long-range) component of the Coulomb drag. Finally, we have approximated the potential in the inversion layer as a triangular-well. This approximation is likely to be satisfactory at the large electron sheet densities of interest, but it will cause additional inaccuracies in the opposite limit of low $n_s$.

It would be interesting to support the results of our calculation with experimental evidence. Unfortunately, we have already alluded to the many experimental and processing complications which hamper a fair comparison. One could claim that, at least at present, the use of high-$\kappa$ insulators has indeed resulted in disappointing performance in those few instances in which high-$\kappa$-based MOS transistors have been made in order to measure effective electron mobilities. Ragnarsson *et al.*[38] have reported a peak mobility of 266 $\mathrm{cm}^2$/Vs for $n$MOSFET fabricated using aluminum gates and $Al_2O_3$ films of 'equivalent' thickness $t_{eq} \approx 2.9$ nm. Similarly, Qi and co-workers[39] have measured low mobilities when using 1.6 nm-thick $ZrSiO_4$ and 2.5 nm-thick $ZrO_2$ films, the former appearing to be about 40% better. Even lower values have been observed for other $ZrSiO_4$ films[31], and even for AlN films[40]. While some of these observations seem to agree quite nicely with our results (AlN being an exception we shall discuss shortly), it should be kept in mind that our calculations assume an ideal scenario: Perfectly stoichiometric films with no charges, electron traps (and the associated hysteresis) or interfacial layers. On the contrary, the structure or even the composition of the insulator itself is often unknown with the required accuracy. Charging effects, almost always seen, make it for a difficult, often impossible, accurate determination of the mobility (since an accurate determination of $n_s$ becomes a hard task). Moreover, interfacial $SiO_2$ (or $Si_3N_4$) layers are almost always present. On the one hand this changes substantially the theoretical picture, with the additional complication arising from the coupling of the optical modes of two insulator and the presence of an additional interface (in Sec. IV we estimate these effects in a simplified situation). On the other hand, the structural property of the interface, and not SO scattering, may dominate the experimental situation. This is probably the case for AlN-based MOSFETs, in which the $Si_3N_4$ interfacial layer, with the well-known associated electron traps and instabilities, may completely mask the effects we are trying to observe. In conclusion, it is fair to say that, at least at present, we only have 'suggestive' and 'circumstantial' experimental evidence supporting our results. But no quantitative conclusions should be drawn.

## References


[1] D. E. Kotecki, Integrated Ferroelectrics **16**, 1 (1996).
[2] T. Ohmi, K. Sekine, R. Kaihara, Y. Sato, Y. Shirai, and M. Hirayama, in *Material Research Society, Symposium Proceedings Volume 567*, H. R. Huff, C. A. Ritter, M. L. Green, G. Lukovsky, and T. Hattori editors (MRS, Warrendale, Pennsylvania, 1999), p.3.
[3] S. Q. Wang and G. D. Mahan, Phys. Rev. B **6**, 4517 (1972).
[4] K. Hess and P. Vogl, Solid State Comm. **30**, 807 (1979)
[5] B. T. Moore and D. K. Ferry, J. Appl. Phys. **51**, 2603 (1980).
[6] M. V. Fischetti and S. E. Laux, Phys. Rev. B **48**, 2244 (1993).
[7] M. V. Fischetti, J. Appl. Phys. **89**, 1232 (2000).
[8] M. V. Fischetti and S .E. Laux, J. Appl. Phys. **89**, 1205 (2000).
[9] We neglect here additional complications which may arise when dealing with layers of thickness comparable to the lattice constant or the size of the molecular bonds, such as localized/quantized phonon modes and electronic states.
[10] As explained in Ref. 7, scattering with the substrate-plasmon component of the excitations is assumed to have no effect on the electron momentum relaxation rate, and so on the mobility, since it involves no direct loss of momentum by the 2DEG.
[11] M. E. Kim, A. Das, and S. D. Senturia, Phys. Rev. B **18**, 6890 (1978).
[12] E. A. Stern and R. A. Ferrel, Phys. Rev. **120**, 130 (1960).
[13] C. Kittel, *Quantum Theory of Solids* (Wiley, New York, 1963).
[14] T. Ando, A. B. Fowler, and F. Stern, Rev. Mod. Phys. **54**, 437 (1982).
[15] S. Takagi, A. Toriumi, M. Iwase, and H. Tango, IEEE Trans. Electron Device **41**, 2357 (1994)
[16] S. Villa, A. Lacaita, L. M. Perron, and R. Bez, IEEE Trans. Electron Device **45**, 110 (1998).
[17] See, for example, P. Balk, S. Ewert, S. Shmidtz, and A. Steffen, J. Appl. Phys. **69**, 6510 (1991).
[18] E. Ruiz, S. Alvarez, and P. Alemany, Phys. Rev. B **49**, 7115 (1994).
[19] P. J. Chen, M. L. Colaianni, and J. T. Yates, Phys. Rev. B **41**, 8025 (1990).
[20] D. A. Neumayer and E. Cartier, J. Appl. Phys. **90**, 1801 (2001).
[21] D. A. Kleinman and W. G. Spitzer, Phys. Rev. **125**, 16 (1962).
[22] J. F. Scott and S. P. S. Porto, Phys. Rev. 161, 903 (1967).
[23] F. L. Galeener and G. Lucovsky, Phys. Rev. Lett. **37**, 1474 (976).
[24] P. Umari, A. Pasquarello, and A. Dal Corso, Phys. Rev. B **63**, 94305 (2001).
[25] B. G. Frederick, G. Apai, and T. N. Rhodin, Phys. Rev. B **44**, 1880 (1991).
[26] I. Gorczyca, N. E. Christensen, E. L. Peltzer y Blanca, and C. O. Rodriguez, Phys. Rev. B **51**, 11936 (1995).
[27] S. Desgreniers and K. Lagarec, Phys. Rev. B **59**, 8467 (1999).
[28] G. Morell, R. S. Katiyar, D. Torres, S. E. Paje, and J. Llopis, J. Appl. Phys. **81**, 2830 (1997).
[29] C. Pecharromán, M. Ocaña, and C. J. Serna, J. Appl. Phys. **80**, 3479 (1996).
[30] A. P. Mirgorodsky, M. B. Smirnov, P. E. Quintard, and T. Merle-Méjan, Phys. Rev. B **52**, 9111 (1995).
[31] A. C. Callegari, private communication.
[32] C. M. Philippi and K. S. Mazdiasni, J. Am. Ceram. Soc. **54**, 254 (1971).
[33] L. Kang, B. H. Lee, W.-J. Qi, Y. Jeon, R. Nieh, S. Gopalan, and J. C. Lee, IEEE Electron Dev. Lett. **21**, 181 (2000)

[34] M. Alvisi, S. Scaglione, S. Martelli, A. Rizzo, and L. Vasanelli, Thin Solid Films **354**, 19 (1999).
[35] T. Nishide, S. Honda, M. Matsuura, and M. Ide, Thin Solid Films **371**, 61 (2000).
[36] G.-M. Rignanese, X. Gonze, and A. Pasquarello, Phys. Rev. B **63**, 104305 (2001).
[37] J. D. Barrie and E. L. Fletcher, J. Vac. Sci. Technol. **A 14**, 795 (1996).
[38] L.-Å. Ragnarsson, S. Guha, N. A. Bojarczuk, E. Cartier, M. V. Fischetti, K. Rim, and J. Karasinski, *Electrical Characterization of* $Al_2O_3$ *n-channel Metal-Oxide-Semiconductor Field-Effect Transistors with Aluminum Gates*, unpublished (2001).
[39] W-J. Qi, R. Nieh, B. H. Lee, K. Onishi, L. Kang, Y. Jeon, J. C. Lee, V. Kaushik, B-Y. Prabhu, K. Eisenbeiser, and J. Finder, in 2000 Symp. on VLSI Technol. Dig., p. 40.
[40] L.-Å. Ragnarsson, private communication.